ACS Catalysis

Research Article

pubs.acs.org/acscatalysis

Catalytic Pathways and Kinetic Requirements for Alkanal Deoxygenation on Solid Tungstosilicic Acid Clusters

Fan Lin and Ya-Huei Cathy Chin*

Department of Chemical Engineering and Applied Chemistry, University of Toronto, Toronto M5S 3E5, Canada

Ⓢ *Supporting Information*

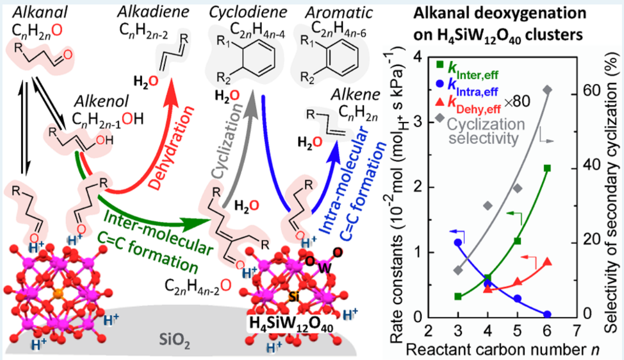

ABSTRACT: Kinetic measurements and acid site titrations were carried out to interrogate the reaction network, probe the mechanism of several concomitant catalytic cycles, and explain their connection during deoxygenation of light alkanals ($C_nH_{2n}O$, $n = 3-6$) on tungstosilicic acid clusters ($H_4SiW_{12}O_{40}$) that leads to hydrocarbons (e.g., light alkenes, dienes, and larger aromatics) and larger oxygenates (e.g., alkenals). The three primary pathways are (1) intermolecular C═C bond formation, which couples two alkanal molecules in aldol-condensation reactions followed by rapid dehydration, forming a larger alkenal ($C_{2n}H_{4n-2}O$), (2) intramolecular C═C bond formation, which converts an alkanal directly to an n-alkene (C_nH_{2n}) by accepting a hydride ion from H donor and ejecting a H_2O molecule, and (3) isomerization−dehydration, which involves self-isomerization of an alkanal to form an allylic alcohol and then rapid dehydration to produce an n-diene (C_nH_{2n-2}). The initial intermolecular C═C bond formation is followed by a series of sequential intermolecular C═C bond formation steps; during each of these steps an additional alkanal unit is added onto the carbon chain to evolve a larger alkenal ($C_{3n}H_{6n-4}O$ and $C_{4n}H_{8n-6}O$), which upon its cyclization−dehydration reaction forms hydrocarbons ($C_{tn}H_{2tn-2t}$, $t = 2-4$, including cycloalkadienes or aromatics). The intermolecular and intramolecular C═C bond formation cycles are catalytically coupled through intermolecular H-transfer events, whereas the intermolecular C═C bond formation and isomerization−dehydration pathways share a coadsorbed alkanal−alkenol pair as the common reaction intermediate. The carbon number of alkanals determines their hydride ion affinities, the stabilities of their enol tautomers, and the extent of van der Waals interactions with the tungstosilicic clusters; these factors influence the stabilities of the transition states or the abundances of reaction intermediates in the kinetically relevant steps and in turn the reactivities and selectivities of the various cycles.

KEYWORDS: *alkanal, deoxygenation, tungstosilicic acid, polyoxometalate cluster, Brønsted acid, aldol condensation, hydride transfer, dehydration*

1. INTRODUCTION

Fast pyrolysis of lignocellulosic biomass produces light oxygenates with less than or equal to six carbon atoms.[1,2] Contained within the light oxygenate fraction are alkanals, such as hydroxyacetaldehyde and furfural, which account for ~20 wt % of the organic fraction.[2,3] These alkanals react on solid Brønsted acid catalysts (e.g., H-ZSM-5,[4−7] H-MOR,[6] and H-FAU[6,7] zeolites) via a series of aldol condensation and dehydration reactions, through which they augment their size by creating intermolecular carbon−carbon linkages. The condensation reactions may occur multiple times to further augment the carbon chain until the eventual intramolecular carbon−carbon bond formation, followed by dehydration, dehydrogenation, and transalkylation to evolve diverse aromatics. As an example, deoxygenation of propanal (C_3H_6O) on H-ZSM-5 zeolites at 673 K leads predominantly to C_6-C_{10+} aromatics with carbon selectivities between 42% and 53%.[8,9]

The mechanism for the initial aldol condensation on solid acid catalysts (H-MFI[10,11] and H-Y[12]) has been well established, but few studies have addressed the sequential reactions that lead to the formation of larger olefinic or aromatic products. Propanal reactions on H-ZSM-5 zeolites involve self-condensation and dehydration steps that form the dimeric species (2-methyl-2-pentenal, $C_6H_{10}O$), which undergo sequential cross condensation with another propanal to produce trimeric species (2,4-dimethyl-2,4-heptadienal, $C_9H_{14}O$), before their ring closure and dehydration to evolve C_9 aromatics.[8,9] These C_9 aromatics then undergo secondary transalkylation steps that shuffle their alkyl groups via carbenium ion transfer[13] and result in C_6-C_{9+} aromatics.[8,9]

Other reactions occur concurrently with the intermolecular carbon−carbon bond formation and ring closure reactions.

Received: June 29, 2016
Revised: August 13, 2016
Published: August 18, 2016

DOI: 10.1021/acscatal.6b01832
ACS Catal. 2016, 6, 6634−6650

Alkanals ($C_nH_{2n}O$) may remove their oxygen via a direct dehydration route, which forms the corresponding dienes (C_nH_{2n-2}).[14−17] In fact, previous studies have shown that 2-methylbutanal dehydration on borosilicate zeolite[14] or aluminum phosphate ($AlPO_4$)[16,17] leads to isoprene,[14,16,17] whereas 2-methylpentanal dehydration on aluminosilicate zeolite (H-Y) leads to 2-methylpenta-1,3-diene,[14] as viable routes for synthesizing polymer precursors. These alkanal dehydration reactions were proposed[17] to occur via a common allylic alcohol intermediate: 2-methylbutanal reactions catalyzed by BPO_4 and $AlPO_4$ catalysts (598−673 K) form isoprene and methyl isopropyl ketone; under similar conditions, both 2-methylbutanal and methyl isopropyl ketone reactions give similar yields to isoprene on $AlPO_4$ (54% vs 49% at 673 K). Therefore, these reactions must involve a common allylic intermediate for the interconversion between isoprene and methyl isopropyl ketone.[17] In addition, 2-methyl-2-buten-1-ol reaction on BPO_4 (383 K) forms 2-methylbutanal, methyl isopropyl ketone, and isoprene with selectivities of 11%, 46%, and 43%, respectively. These allylic alcohols, alkanals, ketones, and isoprenes can interconvert with the allylic alcohol as the intermediate.[17] During alkanal dehydration, the formation of allylic alcohol is likely the initial kinetically relevant step, because the 2-methyl-2-buten-1-ol remains undetected during 2-methylbutanal dehydration (BPO_4 and $AlPO_4$) at 598−673 K.[17]

A separate reaction for alkene formation from alkanal may also occur, as reported previously for alkanal reactions on H-ZSM-5 zeolite.[8,11] Propanal reactions on H-ZSM-5 zeolite at 673 K produce significant amounts of C_1-C_3 light gases (43−53% carbon selectivities) and predominantly propene.[8] In fact, reactions of $C_nH_{2n}O$ alkanal (n = 3−5) on H-ZSM-5 zeolites produce almost exclusively C_nH_{2n} alkenes within the alkene product fraction.[11] The alkene formation likely occurs via a direct hydrogen transfer step, during which a protonated alkanal accepts a hydride ion, followed by dehydration and desorption as alkene, leaving its carbon backbone intact.[18]

Several catalytic routes occur concomitantly, which result in larger oxygenates, alkenes, and aromatics as well as light alkenes and dienes during alkanal deoxygenation on solid Brønsted acid catalysts. Their individual rates, kinetic requirements, and the kinetic connection between these pathways have, however, remained largely unresolved. The ambiguity of the catalytic pathways and the associated mechanism are caused, in large part, by the complexity of the reaction systems, which appear to involve condensation of two alkanals, dehydration of a single alkanal, shuffling of H atoms from products to reactants, and various secondary ring closure and transalkylation reactions. Probing these inherently complex pathways on catalysts containing diverse site structures further complicates the rate data interpretation, because rates of these steps are expected to vary with the site structures and their thermodynamic properties.

Here, we probe the catalytic pathways of alkanal deoxygenation with kinetic and chemical titration strategies, after isolating the kinetic contributions of acid site and site environment. We focus on the deoxygenation chemistry of straight-chain alkanals with three to six carbon atoms ($C_nH_{2n}O$, n = 3−6), carried out on tungstosilicic acid clusters ($H_4SiW_{12}O_{40}$) with well-defined structures. Such clusters contain isolated H^+ sites without the local molecular confinement typically found in microporous crystalline materials. Through quantitative kinetic studies, we probe the reaction pathways by systematically examining the primary and secondary reactions and also by decoupling the rate contributions from the various catalytic routes. Specifically, we establish the kinetic correlation among the three primary pathways during C_3-C_6 alkanal ($C_nH_{2n}O$) deoxygenation on Brønsted acid sites of $H_4SiW_{12}O_{40}$ clusters that lead to larger alkenals ($C_{2n}H_{4n-2}O$) through bimolecular C=C bond formation, light alkenes (C_nH_{2n}) via H transfer and dehydration, and dienes (C_nH_{2n-2}) from direct dehydration reactions. These rates and selectivities on tungstosilicic acid clusters differ from those on microporous crystalline materials (e.g., H-MFI[11] and H-FAU[18]); specifically, the tungstosilicic acid clusters exhibit much higher selectivities toward alkanal coupling than H transfer and direct alkanal dehydration reactions and less extent of cyclization and transalkylation reactions, because of the lack of local H^+ site confinements and the different extents of van der Waals interaction in comparison to zeolites. Our approach provides simple explanations to the apparent complex reaction system and correlates thermochemical properties (e.g., hydride ion affinities and heats of adsorption) to rates and selectivities during deoxygenation reactions.

2. EXPERIMENTAL METHODS

2.1. Preparation and Characterizations of $H_4SiW_{12}O_{40}$ Clusters Dispersed on SiO_2 Support. $H_4SiW_{12}O_{40}/SiO_2$ catalysts (loading amount 0.075 $\mathrm{mmol}_{H_4SiW_{12}O_{40}}\ {g_{SiO_2}}^{-1}$) were prepared by the incipient wetness impregnation method. The SiO_2 support (GRACE chromatographic grade, Code 1000188421, surface area 330 $m^2\ g^{-1}$, particle size <75 μm, pore volume 1.2 $cm^3\ g^{-1}$) was heated in air (Linde, zero grade) at 0.17 K s^{-1} to 773 K and then maintained at 773 K for 5 h. The treated SiO_2 support was impregnated with a solution at a liquid to solid ratio of 1.2 $cm^3\ {g_{SiO_2}}^{-1}$, prepared by dissolving $H_4SiW_{12}O_{40}$ as received (Sigma-Aldrich, reagent grade, CAS #12027-43-9) in ethanol (Sigma-Aldrich, >99.5%, anhydrous). The sample was then held in a closed vial for 24 h and then treated in flowing dry air (Linde, zero grade, 0.1 $cm^3\ (g_{cat}\ s)^{-1}$) at 0.017 K s^{-1} to 323 K and maintained at 323 K for 24 h.

The ratio of Brønsted to Lewis acid sites on $H_4SiW_{12}O_{40}/SiO_2$ catalysts was determined by an infrared spectroscopic study of pyridine adsorption at 473 K. The Brønsted to Lewis site ratio was found to be 14.7, as shown in section S1 in the Supporting Information.[19] The total acid site densities (including Brønsted and Lewis sites) were determined by isothermal chemical titration with pyridine followed by temperature-programmed desorption (TPD) in flowing He. Catalyst powders (150 mg) were loaded into a microcatalytic quartz reactor (9.5 mm inner diameter), supported on a coarse quartz frit. The catalyst powders were treated in situ under flowing He (Linde, grade 5.0, 0.83 $cm^3\ s^{-1}$) at a constant heating rate of 0.083 K s^{-1} to 473 K. As the reactor temperature reached and was maintained isothermally at 473 K, pyridine (Sigma-Aldrich, >99.9%, CAS #110-86-1) was introduced at 3.42×10^{-8} mol s^{-1} through a gastight syringe (SGE, Model 006230, 0.25 cm^3) into a vaporization zone maintained at 391 K and located at the upstream of the reactor, within which pyridine was evaporated and mixed with a flowing He stream (Linde, grade 5.0, 0.83 $cm^3\ s^{-1}$). The amount of pyridine in the effluent stream was quantified using a flame ionization detector (FID) in a gas chromatograph (Agilent, 7890A). Pyridine adsorption was completed when the molar flow rate of pyridine

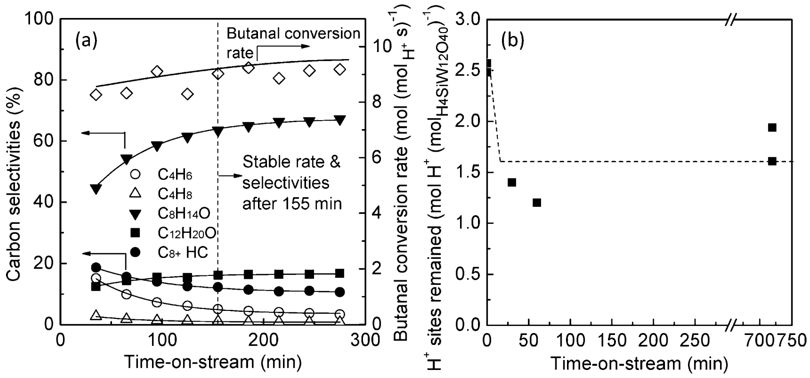

Figure 1. (a) Overall butanal (C_4H_8O) conversion rates (◇) and carbon selectivities for C_4H_6 (○), C_4H_8 (△), $C_8H_{14}O$ (▼), $C_{12}H_{20}O$ (■), and C_{8+} hydrocarbons (labeled C_{8+} HC, ●) as a function of time on stream during butanal reactions on $H_4SiW_{12}O_{40}$ clusters at 573 K (butanal pressure 1.1 kPa, 0.045 $mol_{butanal}$ $(mol_{H^+}\ s)^{-1}$, butanal conversion 18−24%). (b) H^+ site density, expressed as the number of H^+ sites per $H_4SiW_{12}O_{40}$ cluster, remaining after butanal reactions at 573 K plotted as a function of time on stream (butanal pressure 1.1−4.4 kPa, space velocity 0.045−0.18 $mol_{butanal}$ $(mol_{H^+}\ s)^{-1}$).

in the effluent stream became identical with that of the feed stream, at which point the isothermal chemical titration step was completed. The reactor was subsequently purged in flowing He (Linde, grade 5.0, 0.83 $cm^3\ s^{-1}$) at 473 K for 30 min. The He flow rate was then adjusted to 0.17 $cm^3\ s^{-1}$, and the temperature was increased linearly from 473 to 923 K at 0.033 K s^{-1}. The amount of pyridine desorbed into the effluent stream as a function of time (which was also related to the temperature) was quantified using the FID detector. The total acid site densities were determined on the basis of the pyridine uptakes during the chemical titration step as well as that of pyridine desorbed during the TPD, by assuming a pyridine to acid site molar ratio of unity. Both methods gave consistent results (0.169 ± 0.006 $mmol_{acid\ site}\ g_{cat}^{-1}$); thus, the Brønsted site density is 0.159 ± 0.006 $mmol_{H^+}\ g_{cat}^{-1}$ based on the Brønsted-to-Lewis site ratio determined by the infrared spectra of pyridine adsorption. The turnover rates of alkanal reactions reported in this work were calculated on the basis of the initial H^+ site density on the fresh $H_4SiW_{12}O_{40}/SiO_2$ catalysts.

The H^+ site titration with alkanal ($C_nH_{2n}O$, n = 3−6) was performed using a procedure similar to the pyridine titration. A 50 mg portion of the catalyst powder was loaded in the microcatalytic quartz reactor. The samples were treated under flowing He (Linde, grade 5.0, 0.83 $cm^3\ s^{-1}$) by heating to 473 K at 0.083 K s^{-1}, held for 0.5 h at 473 K, and then cooled to 348 K. The alkanal (propanal (Sigma-Aldrich, Kosher grade, ≥97%, CAS #123-38-6), butanal (Sigma-Aldrich, puriss grade, ≥99%, CAS #123-72-8), pentanal (Sigma-Aldrich, 97%, CAS #110-63-3), or hexanal (Sigma-Aldrich, ≥98%, CAS #66-25-1)) was introduced at 1.7×10^{-8} mol s^{-1} through a gastight syringe (SGE, Model 006230, 0.25 cm^3) into a vaporization zone, which was maintained at the boiling point of the alkanal, within which the alkanal was evaporated and mixed with a flowing He stream (Linde, grade 5.0, 0.83 $cm^3\ s^{-1}$). The amount of alkanal in the effluent stream was quantified using a flame ionization detector (FID) in a gas chromatograph (Agilent, 7890A). Alkanal adsorption was completed when the molar flow rate of alkanal in the effluent stream became identical with that of the feed stream.

2.2. Rate and Selectivity Assessments for Alkanal Deoxygenation on $H_4SiW_{12}O_{40}$ Polyoxometalate Clusters. Reactions of alkanals ($C_nH_{2n}O$, n = 3−6) or 2,4-heptadienal ($C_7H_{10}O$) on $H_4SiW_{12}O_{40}/SiO_2$ catalysts were carried out in a fixed bed microcatalytic quartz reactor (9.5 mm inner diameter) with plug-flow fluid dynamics at 573 K. The reactor was contained within a resistively heated furnace with its temperature controlled by a digital feedback controller (Omega, CN3251). Inside the quartz reactor, catalyst powders (25 or 50 mg) were supported on a coarse quartz frit and the bed temperature was recorded using a K-type thermocouple placed at the center (in both the axial and radial directions) of the catalyst bed. Catalysts were treated in situ under flowing He (Linde, grade 5.0, 4.16−33.3 $cm^3\ (g_{cat}\ s)^{-1}$), by heating at 0.167 K s^{-1} to the reaction temperature (573 or 623 K) prior to rate and selectivity measurements. Propanal (Sigma-Aldrich, Kosher grade, ≥97%, CAS #123-38-6), butanal (Sigma-Aldrich, puriss grade, ≥ 99%, CAS #123-72-8), pentanal (Sigma-Aldrich, 97%, CAS #110-63-3), hexanal (Sigma-Aldrich, ≥98%, CAS #66-25-1), or 2,4-heptadienal (Sigma-Aldrich, ≥90%, CAS #4313-03-5) was introduced into a vaporization zone located upstream of the reactor through a gastight syringe (Hamilton, Gastight 1105, 5 mL, or SGE, Model 006230, 0.25 cm^3), mounted on a syringe infusion pump (KD Scientific, LEGATO 100). In the vaporization zone, the reactant was evaporated and mixed with a flowing He stream (Linde, grade 5.0, 4.16−33.3 $cm^3\ (g_{cat}\ s)^{-1}$). The partial pressure of reactants was maintained at a constant value between 1.1 and 10 kPa by controlling the liquid infusion rate of the syringe infusion pump. The mixture was fed to the reactor via heated transfer lines held at 473 K. The reactor effluent stream was kept above 473 K and quantified with an online gas chromatograph (Agilent, 7890A) and mass spectrometer (Agilent, 5975C) equipped with two capillary columns of (i) Agilent HP-5MS (19009lS-433, 30 m, 0.25 mm i.d., 0.25 μm film) connected to a thermal conductivity detector (TCD) and a flame ionization detector (FID) in series and (ii) HP-5 (19091J-413, 30 m, 0.32 mm i.d., 0.25 μm film) connected to the mass spectrometer. These two capillary columns separated the effluent species in the same order and with very similar retention times. After chromatographic separation, each peak which corresponds to a chemical species was identified by examining its associated mass spectrum and then matching the mass spectrum to the NIST/EPA/NIH mass spectral library. Using this method, peaks corresponding to hydrocarbons (olefins, aromatics, dienes, etc.) and oxygenates (alkenals, alkenones, etc.) were identified. The concentrations of these species were further quantified on the basis of their individual FID signal intensity and FID response factor (determined according to the method established in the

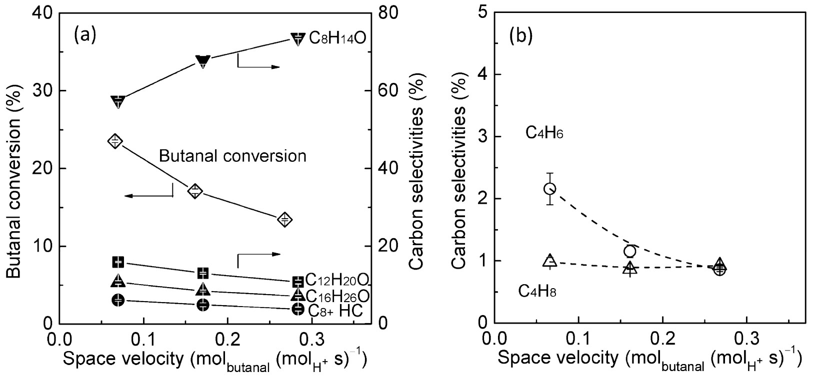

Figure 2. Butanal conversions and carbon selectivities to (a) $C_8H_{14}O$ (▼), $C_{12}H_{20}O$ (■), $C_{16}H_{26}O$ (▲), and C_{8+} hydrocarbons (●, labeled C_{8+} HC, including $C_{4t}H_{6t}$ aromatics (t = 3, 4), cycloalkadienes (t = 2), and $C_{4t}H_{6t+2}$ cycloalkenes (t = 2)) and (b) C_4H_6 (○) and C_4H_8 (△) during butanal (C_4H_8O) reactions on $H_4SiW_{12}O_{40}$ clusters (0.075 mmol$_{H_4SiW_{12}O_{40}}$ g$_{SiO_2}$$^{-1}$) as a function of space velocity at 623 K (1.1 kPa butanal in He, time on stream >155 min, at which stable conversions and selectivities were attained).

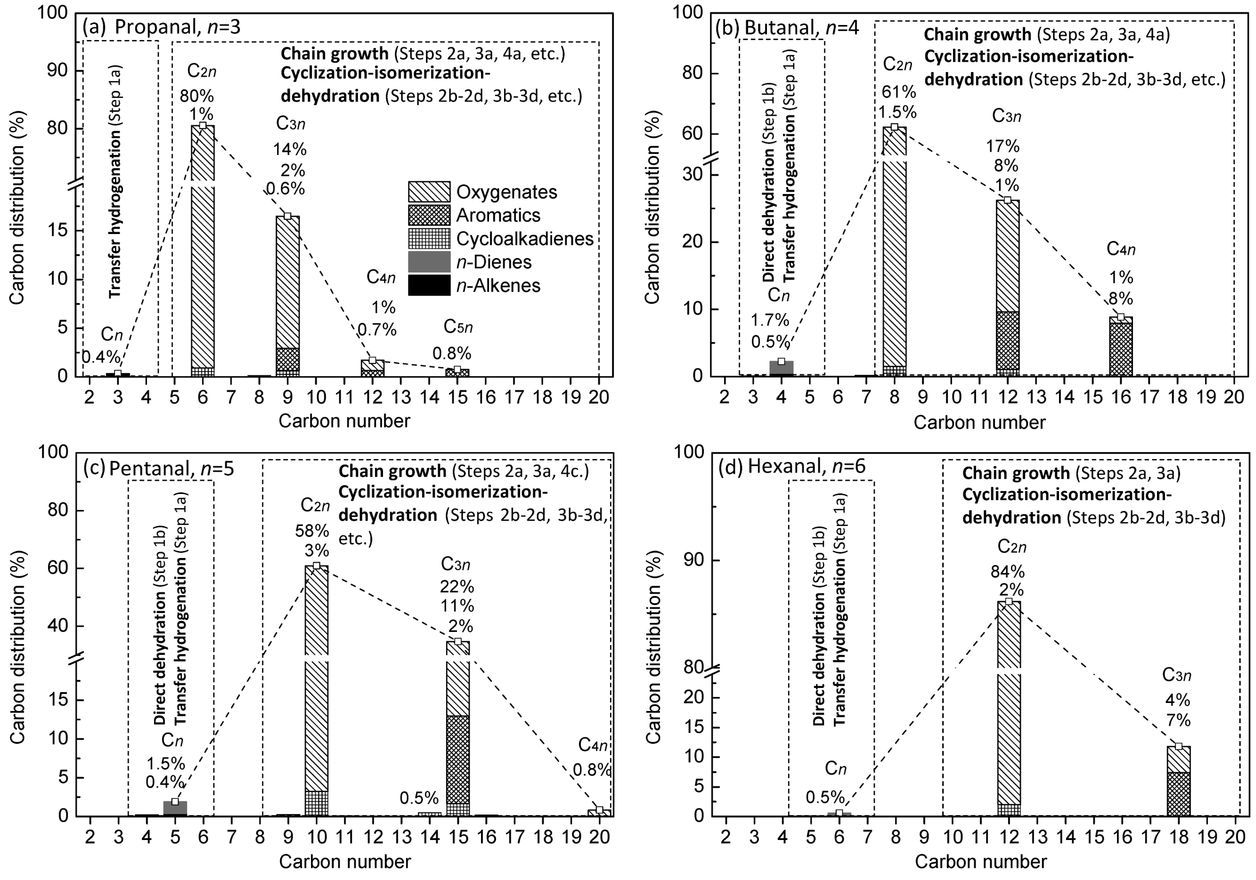

Figure 3. Carbon distributions of the products, including oxygenates (from Steps 2a−2c, 3a−3c, 4a, etc. in Scheme 1), aromatics (from Steps 3d and 3e etc.), cycloalkadienes (from Step 2d), n-dienes (from Step 1b), and n-alkenes (from Step 1a), during (a) propanal, (b) butanal, (c) pentanal, and (d) hexanal reactions on $H_4SiW_{12}O_{40}$ clusters at 573 K (0.075 mmol$_{H_4SiW_{12}O_{40}}$ g$_{SiO_2}$$^{-1}$, space velocity 0.045 mol$_{alkanal}$ (mol$_{H^+}$ s)$^{-1}$, alkanal pressure 1.1 kPa, time on stream 275 min, conversion 17%, 30%, 47%, and 68% for propanal, butanal, pentanal, and hexanal, respectively). See panel (a) for a legend to the bar graph shading.

literature[20]). The CO and CO_2, which could not be detected by FID, were quantified on the basis of their relative mass spectrum signal intensities in comparison with those of the hydrocarbon species (e.g., C_3−C_6 alkenes).

3. RESULTS AND DISCUSSION

3.1. Catalytic Pathways of Alkanal Deoxygenation on $H_4SiW_{12}O_{40}$ Tungstosilicic Acid Dispersed on High-Surface-Area Silica Substrates.

Reactions of straight-chain alkanals ($C_nH_{2n}O$, n = 3−6) on solid Brønsted acid sites at moderate temperatures (473−673 K) and ambient pressure form larger alkenals and their isomers ($C_{tn}H_{2tn-2t+2}O$, n = 3−6, t = 2−4), as well as hydrocarbons including aromatics ($C_{tn}H_{2tn-2t}$, n = 3−6, t = 3, 4), cycloalkadienes ($C_{tn}H_{2tn-2t}$, n = 3−6, t = 2), cycloalkenes ($C_{tn}H_{2tn-2t+2}$, n = 3−6, t = 2), light straight-chain alkenes (C_nH_{2n}, n = 3−6), and dienes (C_nH_{2n-2},

Scheme 1. Pathways for Alkanal ($C_nH_{2n}O$) Chain Growth Resulting in Larger Alkenals (and Their Isomers, $C_{tn}H_{2tn-2t+2}O$, n = 3−6, t = 2, 3) and Hydrocarbons (Including Cycloalkadienes and Aromatics, $C_{tn}H_{2tn-2t}$, n = 3−6, t = 2, 3)[a]

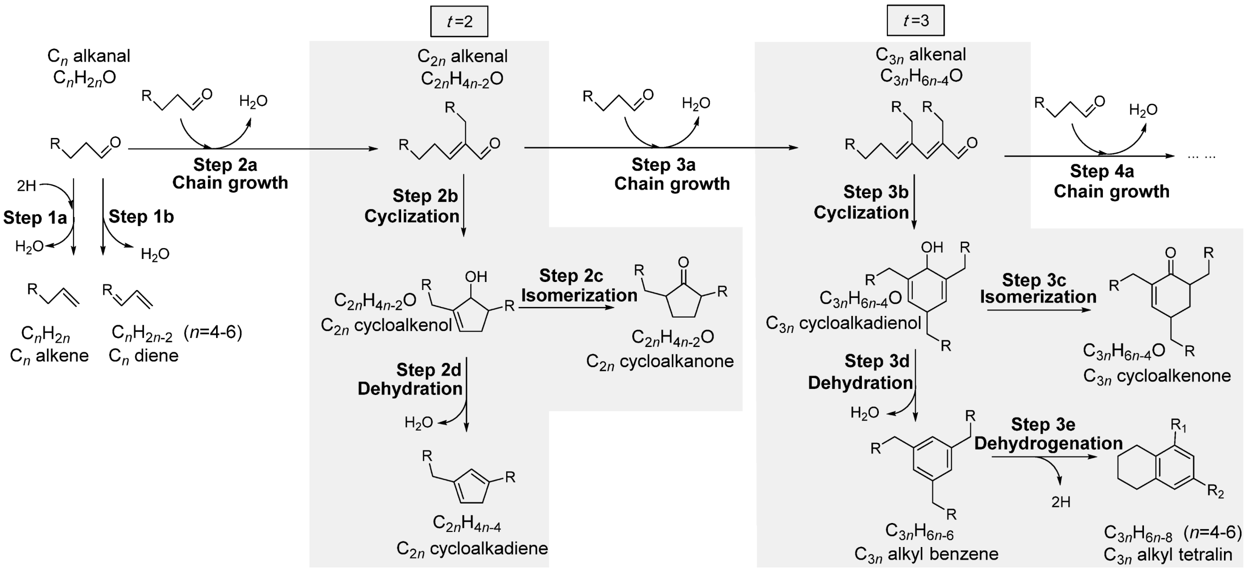

[a] R, R$_1$, and R$_2$ represent either an alkyl group or H.

n = 4−6). The reactions on dispersed $H_4SiW_{12}O_{40}$ clusters (0.075 $mmol_{H_4SiW_{12}O_{40}}$ $g_{SiO_2}{}^{-1}$) at 573 K led to constant alkanal conversion rates and carbon selectivities within experimental errors for reaction times above 155 min, at which stable reactivities were attained, as shown for butanal reactions in Figure 1a. Butanal conversion rates above 155 min remained at 9.1 ± 0.7 mmol $(mol_{H^+}\ s)^{-1}$ and carbon selectivities toward $C_8H_{14}O$, $C_{12}H_{20}O$, C_{8+} hydrocarbons, C_4H_8, and C_4H_6 at 66 ± 1, 16.4 ± 0.2, 11.2 ± 0.6, 0.9 ± 0.05, and 4.1 ± 0.3%, respectively, with the rest (<2%) being minor (e.g., C_7H_{14}) or unidentified products. Pyridine adsorption followed by temperature-programmed desorption and infrared spectroscopic studies of pyridine adsorption gave the H^+ site densities. The H^+ site densities, expressed as the ratio of H^+ sites to $H_4SiW_{12}O_{40}$ clusters, decreased drastically by ~40% (from 2.56 ± 0.09 to 1.54 ± 0.32 mol_{H^+} $(mol_{H_4SiW_{12}O_{40}})^{-1}$) after the initial exposure to butanal reactant (within 30 min) but remained relatively constant at 1.54 ± 0.32 mol_{H^+} $(mol_{H_4SiW_{12}O_{40}})^{-1}$ for the longer reaction duration (30−725 min), as shown in Figure 1b. We have confirmed that the polyoxometalate clusters remain stable at 573 K, because treating the $H_3PW_{12}O_{40}$ in flowing He at 573 K for 3 h only decreases the H^+ site density by 6% (from 3.06 to 2.89 mol_{H^+} $mol_{cluster}{}^{-1}$; Figure S1 in the Supporting Information). Therefore, the marked decrease of the H^+ sites on $H_4SiW_{12}O_{40}$ during the butanal reaction was caused predominantly by the formation of coke and surface acetate (as confirmed from an infrared spectroscopic study reported elsewhere[19]). The surface acetate was formed through alkanal oxidation by the lattice oxygen on polyoxometalate clusters, as detected by the appearance of a 1580 cm^{-1} band, which corresponded to the ν(OCO) symmetric vibration detected in the infrared spectra during butanal adsorption on $H_4SiW_{12}O_{40}$ at 348 K.[19] The coke formation was confirmed from the infrared spectra of $H_4SiW_{12}O_{40}$, taken after the butanal reaction at 573 K for 5 min, which showed that bands at 1580 cm^{-1} resulted from the stretching of the aromatic C═C bond without appearance of the C−H bands (see Figure S2 in the Supporting Information). The coke formation was also confirmed by temperature-programmed oxidation (TPO) carried out on spent $H_4SiW_{12}O_{40}/SiO_2$ catalysts, which showed that 5.2 wt % coke was formed after butanal reactions for 8 h at 573 K (see Section S3 in the Supporting Information). These coke species were formed via butanal condensation and sequential cyclization−dehydrogenation reactions on fresh $H_4SiW_{12}O_{40}$ catalysts.

Figure 2 shows the effects of space velocity on the conversion and carbon selectivities during butanal deoxygenation on $H_4SiW_{12}O_{40}$ clusters at 623 K. As space velocities decreased from 0.26 to 0.07 $mol_{C_4H_8O}$ $(mol_{H^+}\ s)^{-1}$, butanal conversions increased from 13.3% to 23.5%. As the conversion increased, the carbon selectivities toward the $C_8H_{14}O$ fraction, which contained more than 93% 2-ethyl-2-hexenal balanced with a small amount of its isomers, decreased from 73.7% to 57.6%, whereas those toward the larger $C_{12}H_{20}O$, $C_{16}H_{26}O$, and C_{8+} hydrocarbons, which include aromatics (predominantly alkyl benzenes $C_{12}H_{18}$ and $C_{16}H_{24}$), cycloalkadienes (C_8H_{12}), and cycloalkenes (C_8H_{14}), concomitantly increased (Figure 2a). In contrast, carbon selectivities toward butene (C_4H_8) and butadiene (C_4H_6) remained insignificant (<2.5%) throughout the entire range of butanal conversion, as shown in Figure 2b.

These time-dependent rate and selectivity trends remained the same for other alkanals ($C_nH_{2n}O$, n = 3−6) during their deoxygenation reactions on $H_4SiW_{12}O_{40}$ clusters at 573 K. Figure 3 shows the carbon distributions for these different alkanals during their deoxygenation sojourns at steady state (time on stream 275 min). Across the alkanal homologue, the reactions produce chemical species with carbon numbers equaling the multiple of that in the parental alkanal reactants. These selectivity trends indicate that alkanal reactants are incorporated systematically into the alkanal condensation products in a stepwise growth mechanism, which consists of a series of consecutive, intermolecular C═C bond formation events. During each of these C═C bond formation events, the alkanal monomer $C_nH_{2n}O$ is incorporated into and a H_2O molecule is ejected from the growing oxygenate molecule

Scheme 2. Reaction Network for Alkanal ($C_nH_{2n}O$, n = 3−6) Deoxygenation on $H_4SiW_{12}O_{40}$ Clusters Capturing the Intermolecular C=C Bond Formation (*Cycles 1, 1.1,* and *1.2*), Intramolecular C=C Bond Formation (*Cycle 2*), Isomerization−Dehydration (*Cycles* 3 and *3.1*), and the Secondary Cyclization−Dehydration and Dehydrogenation Reactions (*Cyclizations 1*, *2*, *2.1*, and 3), Illustrated with Butanal as an Example

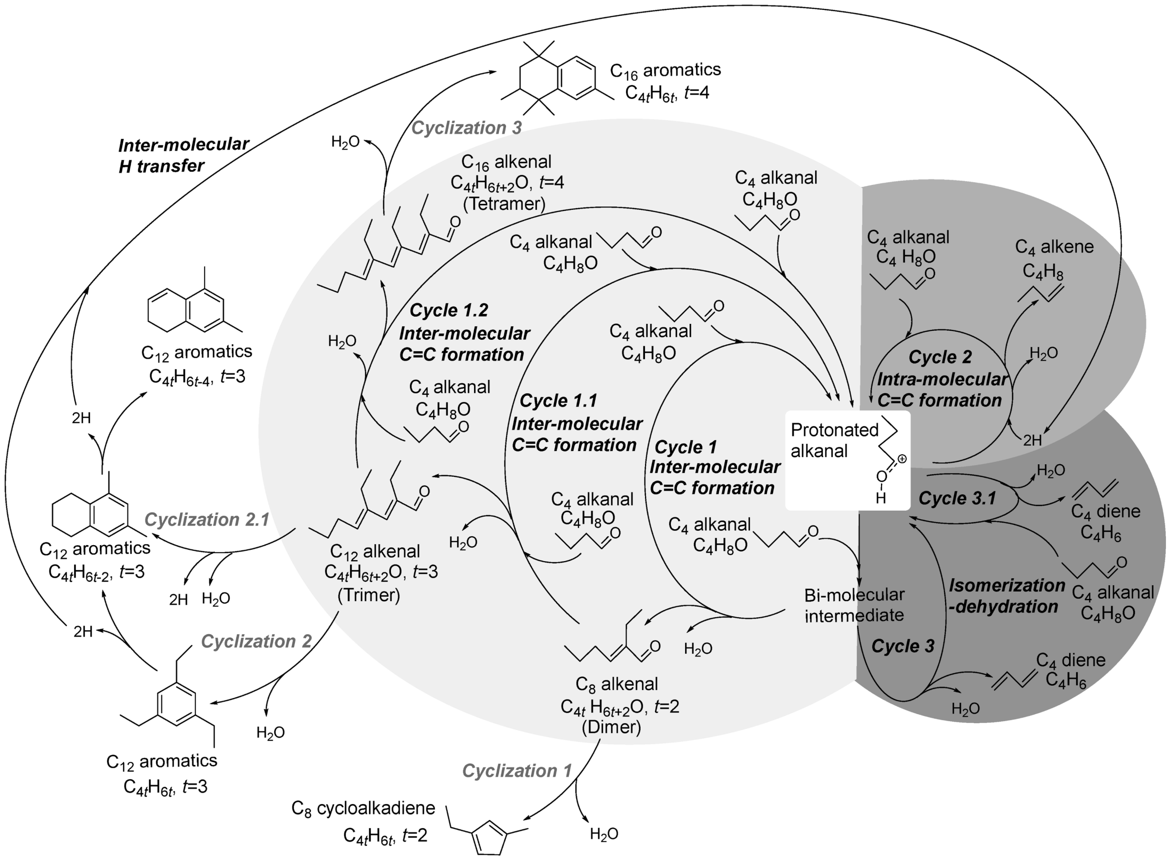

formed from multiple alkanal units, as captured in Scheme 1. Large oxygenates ($C_{tn}H_{2tn-2t+2}O$, n = 3−6, t = 2−4) are produced; these oxygenates contain carbon numbers systematically increased by C_{tn} units (Steps 2a, 3a, and 4a, Scheme 1), where the subscript n denotes the carbon number of the reactant (n = 3−6) and t a positive integer (t = 2−4).

Scheme 1 also captures the sequential reactions of the alkenals ($C_{tn}H_{2tn-2t+2}O$, n = 3−6, t = 2, 3). These alkenals may undergo sequential ring closure, evolving cycloalkenols or cycloalkadienols ($C_{tn}H_{2tn-2t+2}O$, Steps 2b and 3b). The cycloalkenols/cycloalkadienols could either isomerize to cycloalkanones or cycloalkenones ($C_{tn}H_{2tn-2t+2}O$, Steps 2c and 3c) or dehydrate to form cyclodienes or aromatics ($C_{tn}H_{2tn-2t}$, Steps 2d and 3d). The numbers of carbon atoms in the cyclodiene or aromatic product fractions are multiples of the alkanal monomers (tn) and are related to the number of chain growth events, which equals $t-1$ (where t = 2−4). Transalkylation of these C_{tn} hydrocarbons that forms hydrocarbons with $tn-1$ or $tn+1$ carbon atoms (C_{tn-1} and C_{tn+1}) may occur, as reported for alkanal reactions on zeolites,[8,11,18] but the reaction is kinetically insignificant on polyoxometalate clusters, as confirmed from the low carbon selectivities of <1% on $H_4SiW_{12}O_{40}$ clusters (to be discussed in section 3.4). The primary aromatic products (e.g., alkyl benzenes) can undergo dehydrogenation (Step 3e) and evolve alkyl tetralin species (e.g., $C_{3n}H_{6n-8}$, n = 4−6), which are active hydrogen donors required for the light alkene (C_nH_{2n}) formation, as discussed later in this section and in section 3.2. We rule out both decarbonylation and decarboxylation as the predominant routes for oxygen removal, because CO_x formation was below the detectable amounts (<0.03% carbon selectivity) over a broad range of temperature (473−673 K) and residence time (0.045−0.27 $mol_{alkanal}$ $(mol_{H^+}\ s)^{-1}$).

In parallel to the condensation and chain growth reactions, alkanals ($C_nH_{2n}O$, n = 3−6) also convert to light alkenes (C_nH_{2n}, n = 3−6) and dienes (C_nH_{2n-2}, n = 4−6) (Steps 1a and 1b, respectively, Scheme 1). Over 90% of the light alkenes and dienes in their respective product fractions (Figure 3) are molecules with carbon numbers identical with those of their parental alkanal reactants ($C_nH_{2n}/\sum_{m=2}^{m=2n-1}C_mH_{2m}$ > 90% and $C_nH_{2n-2}/\sum_{m=2}^{m=2n-1}C_mH_{2m-2}$ = 100% from $C_nH_{2n}O$ alkanal reactions, n = 3−6, Figure 3). Such near-exclusive selectivities toward these specific alkenes and dienes provide the evidence of their direct formation in reactions that must involve direct hydrogen transfer−dehydration and isomerization−dehydration, respectively, without chain lengthening or contraction.

The space velocity effects (Figure 2) and product distributions (Figure 3) led to the proposed reaction network in Scheme 2, which appears to be general for the deoxygenation of linear alkanals ($C_nH_{2n}O$, n = 3−6) on $H_4SiW_{12}O_{40}$ clusters. Two alkanal molecules undergo a primary, intermolecular C=C bond formation step via an aldol condensation−dehydration route (e.g., butanal condensation forms 2-ethyl-2-hexenal, *Cycle 1*) that results in a dimeric alkenal ($C_{tn}H_{2tn-2t+2}O$, n = 3−6, t = 2, labeled "Dimer").[11] The alkenal ($C_{tn}H_{2tn-2t+2}O$) reacts with another alkanal reactant (*Cycle 1.1*) in a sequential intermolecular C═C bond formation step and, as a result, augments its molecular size, thus evolving a larger alkenal ($C_{tn}H_{2tn-2t+2}O$, n = 3−6, t = 3, labeled "Trimer"). The intermolecular C═C bond formation step may occur again (*Cycle 1.2*), leading to an even larger alkenal ($C_{tn}H_{2tn-2t+2}O$, n = 3−6, t = 4, labeled "Tetramer"). These sequential chain growth events are captured by eqs 1a−1c

$$C_nH_{2n}O + C_nH_{2n}O \rightarrow C_{2n}H_{4n-2}O + H_2O \tag{1a}$$

$$C_{2n}H_{4n-2}O + C_nH_{2n}O \rightarrow C_{3n}H_{6n-4}O + H_2O \tag{1b}$$

$$C_{3n}H_{6n-4}O + C_nH_{2n}O \rightarrow C_{4n}H_{8n-6}O + H_2O \tag{1c}$$

and more generally:

$$tC_nH_{2n}O \rightarrow C_{tn}H_{2tn-2t+2}O + (t-1)H_2O \tag{1d}$$

as also depicted in Scheme 1, Steps 2a−4a, respectively. The dimeric oxygenates ($C_{2n}H_{4n-2}O$, n = 3−6) may undergo concurrent reactions and form cycloalkadienes ($C_{2n}H_{4n-4}$, n = 3−6, t = 2) via cyclization−dehydration and isomerization reactions (*Cyclization 1*). Similarly, larger oxygenates derived from trimeric and tetrameric species ($C_{tn}H_{2tn-2t+2}O$, n = 3−6, t = 3−4) may undergo cyclization−dehydration (*Cyclization 2* and *Cyclization 3*) or cyclization−dehydration−dehydrogenation (*Cyclization 2.1*) reactions that strip all of their oxygen atoms and evolve as aromatic species (including substituted benzenes ($C_{tn}H_{2tn-2t}$) and tetralins ($C_{tn}H_{2tn-2t-2}$), n = 3−6, t = 3, 4).

The primary, intermolecular C═C bond formation event (*Cycle 1*) is kinetically coupled with separate, interdependent catalytic cycles, also shown in Scheme 2, of (i) direct deoxygenation of alkanal (*Cycle 2*, intramolecular C═C formation) that evolves light alkene, during which an intramolecular C═C bond is created, first by H transfer from a H donating agent to a protonated alkanal, followed by dehydration and (ii) competitive isomerization−dehydration via a bimolecular pathway (*Cycle 3*, isomerization−dehydration) that forms light dienes (C_nH_{2n-2}, n = 4−6). These reactions are

$$C_nH_{2n}O + R'H_2 \rightarrow C_nH_{2n} + H_2O + R'$$

$$R'H_2 \text{ represents a H donor} \tag{2a}$$

$$C_nH_{2n}O \rightarrow C_nH_{2n-2} + H_2O \tag{2b}$$

The alkanal isomerization−dehydration could also proceed via a monomolecular route (*Cycle 3.1*, isomerization−dehydration, Scheme 2), which is not kinetically coupled to the pathway of intermolecular C═C bond formation.

Similar deoxygenation pathways are found for C_3−C_6 alkanals (n = 3−6), but their relative rates and selectivities vary systematically with the carbon number n, because of the difference in molecular dimensions, heats of adsorption, and hydride ion affinities, through their influences on the kinetic properties (i.e., activation free energies) of these different pathways. The evidence of catalytic couplings and the mechanistic details of the primary reactions are provided next in sections 3.2 and 3.3.

3.2. Kinetic Coupling of Alkanal Chain Growth, Deoxygenation, and Isomerization−Dehydration Cycles. We describe next the kinetic couplings of alkanal chain growth (*Cycle 1*), intramolecular C═C bond formation (*Cycle 2*), and isomerization−dehydration (*Cycle 3*) catalytic cycles shown in Scheme 2. The reaction stoichiometry for intramolecular C═C bond formation dictates that each alkene formation requires two H atoms ($C_nH_{2n}O + 2H \rightarrow C_nH_{2n} + H_2O$). These hydrogen atoms, in the absence of external H sources, must come from either the reaction intermediates or products. A carbon and hydrogen balance carried out in our previous studies on propanal reactions catalyzed by H-MFI zeolite[11] identifies that aromatic products or precursors to aromatics, typically substituted cyclohexadienes and tetralins produced from the secondary cyclization reactions of larger, unsaturated alkenals (*Cyclization 1*, *Cyclization 2*, *Cyclization 2.1*, and *Cyclization 3*, e.g., 5,6-dimethyl-1,3-cyclohexadiene and 5,7-dimethyltetralin produced in butanal reactions), are the H donors ($R'H_2$) in eq 2a. These substituted cycloalkadienes or tetralins increase their extent of unsaturation via H donation, forming more stable alkyl benzenes or naphthalenes with delocalized π bonds.[21] The catalytic involvement of substituted cycloalkadienes and tetralins was evident from an increase in butene formation rates with cyclohexadiene and tetralin incorporation during butanal reactions on H-FAU zeolites (at 573 K), as reported elsewhere.[18] Indeed, turnover rates for intramolecular C═C bond formation (r_{Intra}) increased linearly with the pressure of the cyclic hydrocarbon products (including cycloalkadienes and aromatics), P_{HC}, for all C_3−C_6 alkanals, as shown in Figure 4a and captured by eq 3:

$$r_{\text{Intra}} = k_{\text{Intra,eff}}P_{\text{HC}} \tag{3}$$

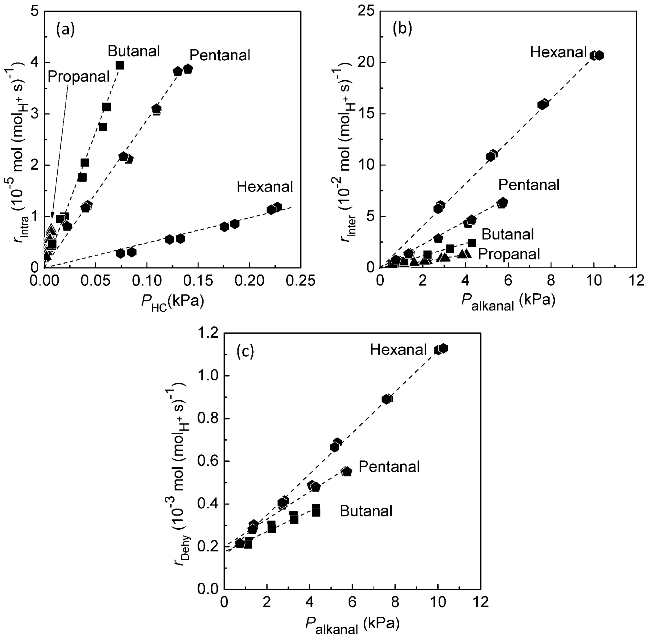

Figure 4. (a) Rates for intramolecular C═C bond formation (r_{Intra}, *Cycle 2* in Scheme 2) as a function of the total pressure of C_8−C_{16} cyclic hydrocarbon product fraction (P_{HC}, including cycloalkadienes and aromatics). (b) Rates for intermolecular C═C bond formation (r_{Inter}, *Cycle 1* in Scheme 2) as a function of alkanal pressure (P_{alkanal}, average alkanal pressure). (c) Rates for isomerization−dehydration (r_{Dehy}, *Cycles 3 and 3.1* in Scheme 2) as a function of alkanal pressure (P_{alkanal}, average alkanal pressure) during the reactions of alkanals ($C_nH_{2n}O$, n = 3−6; propanal (▲), butanal (■), pentanal (⬟), and hexanal (⬢)) on $H_4SiW_{12}O_{40}$ clusters (573 K, 0.045−0.44 mol$_{\text{alkanal}}$ (mol$_{\text{H}^+}$ s)$^{-1}$, time on stream 275−600 min, alkanal conversion 14−17, 26-31, 45−47, and 68−72% for propanal, butanal, pentanal, and hexanal, respectively).

where $k_{\mathrm{Intra,eff}}$ is the effective rate constant for intramolecular C=C bond formation. The H balance[11] and the direct correlations between the rates k_{Intra} and cyclic hydrocarbon pressures (Figure 4a) led us to propose that the intermolecular and intramolecular C=C bond formation cycles (*Cycles 1* and *2*, Scheme 2) are kinetically coupled via the intermolecular hydrogen transfer step.

Next, we probe the catalytic coupling of the initial intermolecular C=C bond formation (*Cycle 1*) and isomerization−dehydration (*Cycle 3*) reactions shown in Scheme 2, which form 2-ethyl-2-hexenal and butadiene, respectively. The rates for intermolecular C=C bond formation (r_{Inter}) and isomerization−dehydration (r_{Dehy}, of both *Cycle 3* and *Cycle 3.1*) measured for butanal reactions on $H_4SiW_{12}O_{40}$ clusters at 573 K are shown in Figure 5 as a function of time on stream.

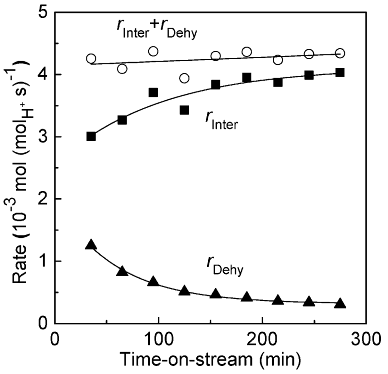

Figure 5. Rates for intermolecular C=C bond formation (r_{Inter}, ■, *Cycle 1* in Scheme 2) and isomerization−dehydration (r_{Dehy}, ▲, *Cycles 3 and 3.1* in Scheme 2) and the combined rate ($r_{\mathrm{Inter}} + r_{\mathrm{Dehy}}$, ○) as a function of time on stream on $H_4SiW_{12}O_{40}$ catalysts (0.075 $\mathrm{mmol_{H_4SiW_{12}O_{40}}\ g_{SiO_2}^{-1}}$) at 573 K (space velocity 0.063 $\mathrm{mol_{butanal}}$ ($\mathrm{mol_{H^+}}$ s)$^{-1}$, butanal conversion 18−24%).

The rates r_{Inter} increase while those of r_{Dehy} concomitantly decrease during the first 155 min of reaction before approaching constant values ($r_{\mathrm{Inter}} = 3.8 \pm 0.2$ mmol ($\mathrm{mol_{H^+}}$ s)$^{-1}$ and $r_{\mathrm{Dehy}} = 0.40 \pm 0.07$ mmol ($\mathrm{mol_{H^+}}$ s)$^{-1}$). Despite changes in these individual rate values during the initial times (<155 min), their combined rates ($r_{\mathrm{Dehy}} + r_{\mathrm{Inter}}$) remain relatively constant (4.4 ± 0.5 mmol ($\mathrm{mol_{H^+}}$ s)$^{-1}$), an indication that the catalytic cycle of intermolecular C=C bond formation (*Cycle 1*) is kinetically coupled with at least one of the isomerization−dehydration pathways (*Cycle 3* and/or *Cycle 3.1*), possibly through sharing common surface intermediates. It has been proposed that alkanal dehydration that forms alkadiene proceeds via an allylic alcohol intermediate upon alkanal isomerization.[17] The alkanal isomerization involves an initial protonation of the carbonyl group at a H^+ site and a sequential β-hydrogen abstraction by a vicinal base site, as proposed for 2-methylbutanal isomerization on BPO_4 and $AlPO_4$ catalysts.[17] These previous studies led us to further postulate that acid−base site pairs are required for alkanal isomerization−dehydration (*Cycles 3* and *3.1*). The anion of tungstosilicic acid cluster ($SiW_{12}O_{40}^{4-}$) has multiple oxygen sites (both bridging and terminal oxygen atoms) that can act as the base sites.[22] As butanal reactions proceed, larger carbonaceous species (e.g., cokes) were deposited on the $H_4SiW_{12}O_{40}$ clusters, covering the oxygen sites. In contrast, the H^+ site density remained relatively stable for reaction times above 30 min (Figure 1b), probably because the alkanals adsorbed at the H^+ sites and protected them from being covered by cokes. The decrease in base sites prevents these shared intermediates, the precursors for the isomerization−dehydration and intermolecular C=C bond formation, from undergoing isomerization−dehydration (*Cycles 3* and *3.1*) and in turn promotes the competitive intermolecular C=C bond formation (*Cycle 1*), as shown in Figure 5, to be discussed in details in sections 3.3 and 3.4.

3.3. Mechanisms for the Formation of Alkenals, Alkenes, and Dienes via Primary Alkanal Reactions on $H_4SiW_{12}O_{40}$ Clusters.

Scheme 3 shows a proposed sequence of elementary steps for the primary alkanal reactions, which includes intermolecular C=C bond formation (Steps G1, A1, and R1.1−R1.5), intramolecular C=C bond formation (Steps A1 and R2.1−R2.4), and isomerization−dehydration via both the bimolecular (Steps A1, R1.1, R3.1a, and R3.2a) and monomolecular (Steps A1, R3.1b, and R3.2b) pathways. Pseudo-steady-state treatments of all reactive intermediates in this sequence and the assumption of protonated butanals as the most abundant surface intermediates lead to a set of rate equations consistent with the observed kinetic dependences for the primary reactions shown in Figure 4 and with the coupling of the various catalytic cycles in Scheme 2, as described next.

Alkanals adsorb on H^+ sites as protonated alkanals ($C_nH_{2n}OH^+$, Step A1, equilibrium constant K_{ads}),[23] as their adsorbed alkenol tautomers (Step A3.1),[24−26] or in their physisorbed equivalence via hydrogen bonds between their oxygen atoms and the H^+ sites (Steps A2.1 and A2.2).[23,24,27] The alkanals and their various surface species are likely in chemical equilibrium, as inferred from previous infrared studies of acetone adsorption on H-ZSM-5[23] that detected both the carbonyl group (1658−1671 cm^{-1}) and the alcohol species (1375 and 880 cm^{-1} for in-plane and out-of-plane O−H bending, respectively). The adsorption weakens the O−H bridging bands of the zeolite at 2850 and 2380 cm^{-1} to different extents as a result of their interactions with the physisorbed and protonated carbonyl groups, respectively.

Protonated carbonyl groups were evident in infrared spectroscopic studies from a red shift of the ν(C=O) band in acetone during its adsorption from 1720 cm^{-1} on Na-ZSM-5 to 1671−1658 cm^{-1} on H-ZSM-5.[23] Adsorbed enols, the surface tautomers, were confirmed from H−D exchange between the H in the adsorbed ^{13}C-2-acetone and the D^+ site and between the D in the adsorbed acetone-d_6 and the H^+ site in ZSM-5 zeolites at ambient temperature.[25] They were also evident from the appearance of the signal at ∼180 ppm in ^{13}C NMR spectra as acetone was adsorbed on H-ZSM-5 and H-Y zeolites between 298 and 453 K.[26] DFT calculations gave an activation barrier of 75.3 kJ mol^{-1} and reaction energy of 31.0 kJ mol^{-1} for the keto−enol tautomerization of acetaldehyde on the H^+ sites in H-ZSM-5 zeolites;[24] thus, the protonated enol is much less stable than the protonated alkanal and is a less abundant surface intermediate. It is noted that the keto−enol tautomerization on H^+ sites (Step A3.1) has a high activation barrier (e.g., $\Delta H_{\mathrm{enol}}^{\ddagger}$ = 75.3 kJ mol^{-1} for acetaldehyde tautomerization on H-ZSM-5);[24] the barrier is even higher in the gas phase (e.g., $\Delta H_{\mathrm{enol}}^{\ddagger}$ = 285 kJ mol^{-1} for acetone tautomerization in the gas phase).[28] The activation enthalpy for keto−enol tautomerization (Step A3.1, $\Delta H_{\mathrm{enol}}^{\ddagger}$) may be much higher than that for aldol condensation (Steps R1.1−R1.3, $\Delta H_{\mathrm{aldol}}^{\ddagger}$). For example, the activation enthalpies for aldol condensation are 8.4 kJ mol^{-1} for 2-propenol and formaldehyde reactions on H-ZSM-5[28] and 27 kJ mol^{-1} for 1-butenol and

Scheme 3. Mechanism for Intermolecular C=C Bond Formation (Steps G1, A1, and R1.1−R1.5, Also Shown as *Cycle 1* in Scheme 2), Intramolecular C=C Bond Formation (Steps A1 and R2.1-R2.4, Also Shown as *Cycle 2* in Scheme 2), and Isomerization−Dehydration via Bimolecular Pathway (Steps R3.1a−R3.2a, also shown as *Cycle 3* in Scheme 2) and Monomolecular Pathway (Steps R3.1b-R3.2b, Also Shown as *Cycle 3.1* in Scheme 2) during Alkanal Reactions on $H_4SiW_{12}O_{40}$ Clusters[a]

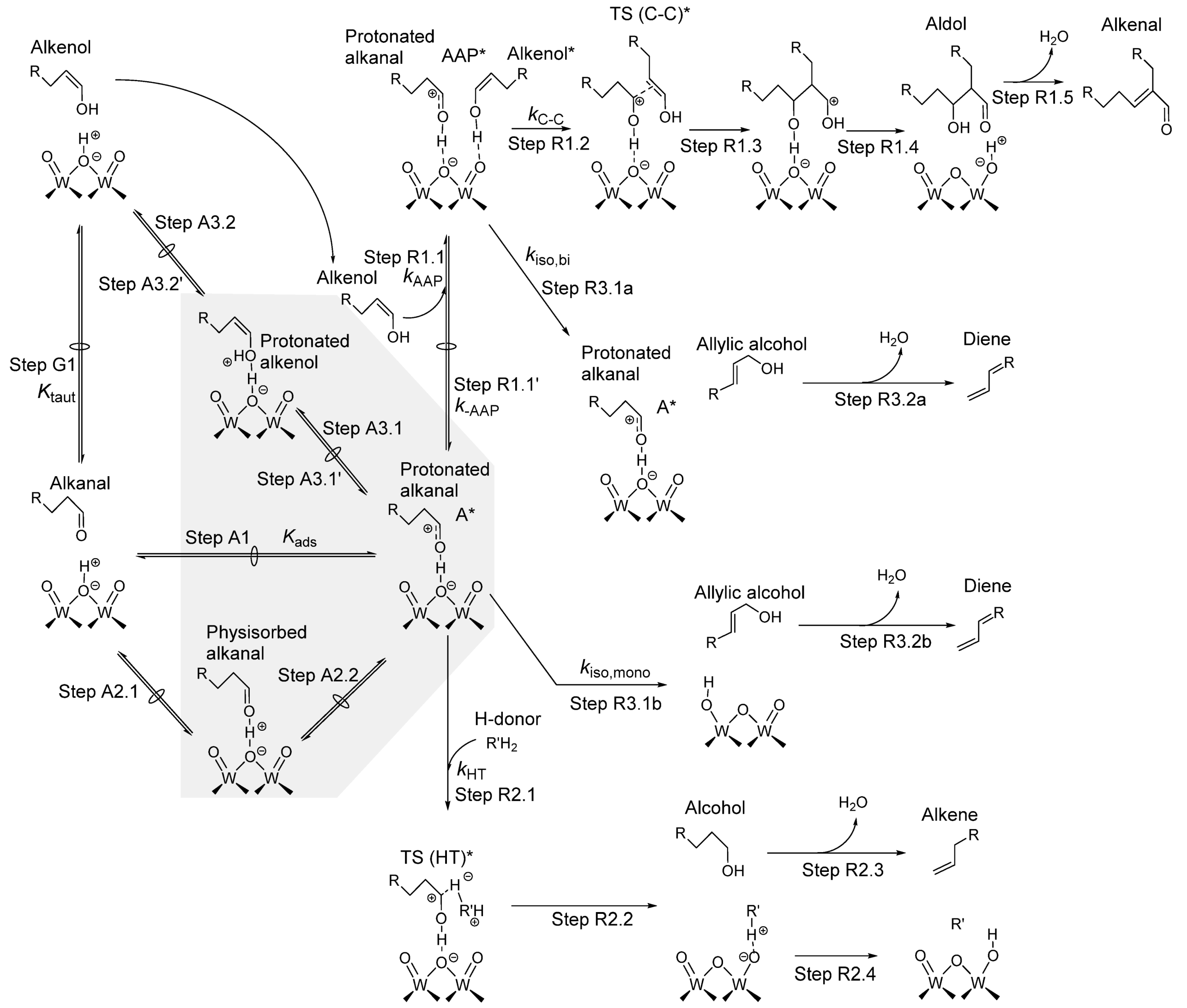

[a] R = H, CH_3, C_2H_5, and C_3H_7 for propanal, butanal, pentanal, and hexanal, respectively; $R'H_2$ represents a H donor.

butanal reactions on Ti−OH sites,[29] on the basis of DFT calculations. The bimolecular aldol condensation step (Steps R1.1−R1.3), however, has an activation entropy more negative than that of the monomolecular keto−enol tautomerization step (Step A3.1). In addition, the aldol condensation (Steps R1.1−R1.3) involves the gaseous enol tautomers with low concentration, whereas the keto−enol tautomerization (Step A3.1) occurs on the protonated alkanals, the most abundant surface species. As a result, Steps R1.1−R1.3 have a lower rate than Step A3.1. For these reasons, the aldol condensation step remains as the rate-limiting step for the intermolecular C=C bond formation and exhibits first-order rate dependence to alkanal pressure, as shown later in this section. Since the alkenol formation via the reversible keto−enol tautomerization (Step A3.1) is not a rate-limiting step, and the alkanal adsorption (Step A1) and alkenol desorption (Step A3.2) steps are all reversible, the reversible keto−enol tautomerization in the gas phase (Step G1) would reach chemical equilibrium during steady-state reactions.

A fraction of the adsorbed alkanals on strong H^+ sites underwent oxidation on the $H_4SiW_{12}O_{40}$ clusters and formed stable surface acetate (not shown in Scheme 3). These acetate species were evident from the appearance of the ν(OCO) symmetric vibrational stretching band at 1580 cm^{-1} during exposure of $H_4SiW_{12}O_{40}$ clusters to butanal at 348 K; the density of surface acetate increased proportionally with the number of strong H^+ sites contained within the clusters, as determined by pyridine-TPD,[19] an indication that these acetate species were formed only on strong H^+ sties. During alkanal reaction at 573 K, these strong H^+ sites were poisoned by the formation of coke (Figure S2 in the Supporting Information), as confirmed from the disappearance of the pyridine desorption peak at 720 K during pyridine-TPD of the spent $H_4SiW_{12}O_{40}$ catalysts (see Figure S5 in the Supporting Information). Therefore, surface acetate species were not present during steady-state reactions at 573 K. The chemical titration of the H^+ sites with C_3−C_6 alkanals at 348 K, a temperature much lower than that of the steady-state reaction, shows near unity alkanal to H^+ site ratios ($C_nH_{2n}O$:H^+ = 1.15, 1.0, 1.08, and 1.05 for n = 3−6, respectively), an indication that the catalytically active H^+ sites not poisoned by cokes are occupied predominantly by protonated alkanal monomers (Step A1, labeled A* in Scheme 3) and their isomers (protonated alkenols and physisorbed alkanals), which are in equilibrium with each other (Steps A3.1 and A2.2), as shown in the shaded area in Scheme 3.

The intermolecular C═C bond formation cycle (*Cycle 1* of Scheme 2) is initiated by keto−enol tautomerization, which transforms a small amount of alkanals to alkenols (Step G1, Scheme 3). As depicted in Scheme 3, we postulate that the alkenol can coadsorb on the lattice oxygen site adjacent to a protonated alkanal and form a coadsorbed alkanal−alkenol pair (labeled AAP*, Step R1.1). Within the AAP* intermediate, nucleophilic attack of the C═C bond in the coadsorbed alkenol ($C_nH_{2n-1}OH^*$, labeled Alkenol*) to the adjacent carbonyl carbon of the protonated alkanal ($C_nH_{2n}OH^+$) (Step R1.2) via a bimolecular transition state (labeled TS(C−C)*) leads to the formation of the aldol $C_{2n}H_{4n}O_2$ (Steps R1.3−R1.4, labeled "Aldol"), which upon sequential dehydration (Step R1.5) forms the alkenal $C_{2n}H_{4n-2}O$. The rate equation for intermolecular C═C formation, derived by considering the nucleophilic attack (Step R1.2) as a kinetically relevant step, is

$$r_{\text{Inter}} = \frac{k_{\text{C-C}}\dfrac{k_{\text{AAP}}(K_{\text{ads}}[\text{H}^+]P_{\text{alkanal}})(K_{\text{taut}}P_{\text{alkanal}})}{k_{-\text{AAP}}+k_{\text{C-C}}+k_{\text{iso,bi}}}}{\underset{(\text{H}^+\text{site})}{[\text{H}^+]} + \underset{(\text{A}^*)}{K_{\text{ads}}[\text{H}^+]P_{\text{alkanal}}} + \underset{(\text{AAP}^*)}{\dfrac{k_{\text{AAP}}(K_{\text{ads}}[\text{H}^+]P_{\text{alkanal}})(K_{\text{taut}}P_{\text{alkanal}})}{k_{-\text{AAP}}+k_{\text{C-C}}+k_{\text{iso,bi}}}} + \underset{(\text{other})}{\alpha}} \tag{4}$$

where K_{ads} and K_{taut} are the equilibrium constants for alkanal adsorption (Step A1) and keto−enol tautomerization (Step G1), respectively, the terms k_{AAP} and $k_{-\text{AAP}}$ are the rate constants for the forward and reverse steps of AAP* formation (Step R1.1), respectively, $k_{\text{C-C}}$ is the rate constant for aldol condensation (Step R1.2), and $k_{\text{iso,bi}}$ is the rate constant for the bimolecular pathway of alkanal isomerization (Step R3.1a). $[\text{H}^+]$ denotes the H^+ site concentration, whereas P_{alkanal} denotes the alkanal pressure. These rate and equilibrium constants are defined in Scheme 3. The relative magnitudes of the denominator terms $K_{\text{ads}}[\text{H}^+]P_{\text{alkanal}}$, $k_{\text{AAP}}(K_{\text{ads}}[\text{H}^+]P_{\text{alkanal}})(K_{\text{taut}}P_{\text{alkanal}})(k_{-\text{AAP}} + k_{\text{C-C}} + k_{\text{iso, bi}})^{-1}$, and α reflect the relative coverages of protonated alkanals (A*), the alkanal−alkenol pairs (AAP*), and other adsorbed species (e.g., alkanal isomers and alkenal products), respectively. The term $K_{\text{ads}}[\text{H}^+]P_{\text{alkanal}}$ is the predominant term in the denominator, when protonated alkanals (A*) are the most abundant surface intermediates, as confirmed from the chemical titration with C_3 to C_6 alkanals. Therefore, eq 4 simplifies to rates that vary linearly with alkanal pressure:

$$r_{\text{Inter}} = \frac{k_{\text{AAP}}k_{\text{C-C}}K_{\text{taut}}}{k_{-\text{AAP}} + k_{\text{C-C}} + k_{\text{iso,bi}}}P_{\text{alkanal}} = k_{\text{Inter,eff}}P_{\text{alkanal}} \tag{5a}$$

$$k_{\text{Inter,eff}} = \frac{k_{\text{AAP}}k_{\text{C-C}}K_{\text{taut}}}{k_{-\text{AAP}} + k_{\text{C-C}} + k_{\text{iso,bi}}} \tag{5b}$$

This first-order dependence for intermolecular C═C bond formation on alkanal pressures (P_{alkanal}) is confirmed for alkanal ($C_nH_{2n}O$, n = 3−6) reactions on $H_4SiW_{12}O_{40}$ clusters at 573 K during steady state, as shown in Figure 4b. The term $k_{\text{AAP}}k_{\text{C-C}}K_{\text{taut}}(k_{-\text{AAP}} + k_{\text{C-C}} + k_{\text{iso, bi}})^{-1}$ in eq 5b reflects the effective rate constant, $k_{\text{Inter,eff}}$. We determine the rate constants (to be discussed in section 3.5) from the rate data using an integral reactor model, because alkanal conversions were higher than 10% (14−17, 26-31, 45−47, and 68−72% for propanal, butanal, pentanal, and hexanal, respectively).

The protonated alkanal may undergo an alternative catalytic cycle (*Cycle 2*, Scheme 2), during which it accepts a hydride ion from a hydride donor (denoted $R'H_2$) in a kinetically relevant step (Step R2.1) to form a carbonium ion transition state with a shared hydride ion, followed by its decomposition (Step R2.2) and kinetically irrelevant dehydration (Step R2.3) to evolve the *n*-alkene, as captured in Scheme 3. Proton donation from the carbenium ion of the hydride donor ($R'H^+$) to the polyoxometalate surfaces (Step R2.4) completes the catalytic cycle and regenerates the H^+ site. This hydride transfer mechanism is similar to those previously studied with DFT calculations between alkanes and protonated alkenes on H_3Si−OH−AlH_2−O−SiH_3 clusters[30−32] and between alkanes to alkoxides in mordenite zeolites.[33] This mechanism leads to the following rate equation for intramolecular C═C bond formation (r_{Intra}):

$$r_{\text{Intra}} = \frac{k_{\text{HT}}K_{\text{ads}}[\text{H}^+]P_{\text{alkanal}}P_{\text{R}'\text{H}_2}}{\underset{(\text{H}^+\text{site})}{[\text{H}^+]} + \underset{(\text{A}^*)}{K_{\text{ads}}[\text{H}^+]P_{\text{alkanal}}} + \underset{(\text{AAP}^*)}{\dfrac{k_{\text{AAP}}(K_{\text{ads}}[\text{H}^+]P_{\text{alkanal}})(K_{\text{taut}}P_{\text{alkanal}})}{k_{-\text{AAP}}+k_{\text{C-C}}+k_{\text{iso,bi}}}} + \underset{(\text{other})}{\alpha}} \tag{6}$$

The denominator terms in this rate equation remain identical with those in eq 4, because both the intermolecular and intramolecular C═C bond formation reactions occur at the same sites. k_{HT} represents the rate constant for the hydride transfer step (Step R2.1), and $P_{\text{R}'\text{H}_2}$ is the partial pressure of the hydride donors. When protonated alkanal (A*) is the most abundant surface intermediate, eq 6 simplifies to rates that depend strictly on the hydride donor pressure:

$$r_{\text{Intra}} = k_{\text{HT}}P_{\text{R}'\text{H}_2} \tag{7}$$

In the absence of external hydrogen sources, the large cyclic hydrocarbon products, including aromatics (e.g., alkylbenzenes and alkyltetralins) and precursors to aromatics (e.g., cycloalkadienes), are the only hydride donors, as they undergo dehydrogenation to further increase their extent of unsaturation. The reactivities of these cyclic hydrocarbon products as H donors vary with their chemical identities, as demonstrated in our previous work.[18] Assuming that β_x is the fraction of a specific H donor $R'H_2(x)$ within the cyclic hydrocarbon products (where x denotes the chemical identity) and $k_{\text{HT},\text{R}'\text{H}_2(x)}$ is the rate constant for transfer hydrogenation between $R'H_2(x)$ and the protonated alkanal, the rate for intramolecular C═C bond formation, r_{Intra}, is

$$\begin{aligned} r_{\text{Intra}} &= \sum_{x=1}^{t} k_{\text{HT},\text{R}'\text{H}_2(x)}P_{\text{R}'\text{H}_2(x)} = \sum_{x=1}^{t} k_{\text{HT},\text{R}'\text{H}_2(x)}\beta_x P_{\text{HC}} \\ &= k_{\text{Intra,eff}}P_{\text{HC}} \end{aligned} \tag{8a}$$

$$k_{\mathrm{Intra,eff}} = \sum_{x=1}^{t} k_{\mathrm{HT,R'H_2}(x)}\beta_x \tag{8b}$$

According to eq 8a, the rate of intramolecular C═C bond formation (r_{Intra}) increases linearly with the partial pressures of cyclic hydrocarbon products (P_{HC}), consistent with the rate dependences shown in Figure 4a. $k_{\mathrm{Intra,eff}}$ is the effective rate constant for intramolecular C═C bond formation, and its value depends on the fractions (β_x) and the hydride transfer rate constants ($k_{\mathrm{HT,R'H_2}(x)}$) of the various H donors ($\mathrm{R'H_2}(x)$, x = 1, 2, ...), as shown in eq 8b. This direct, linear relation between the rates of intramolecular C═C bond formation and the hydrocarbon pressures is found not only for C_3-C_6 alkanal reactions on $H_4SiW_{12}O_{40}$ clusters at 573 K (Figure 4a) but also for butanal reactions on H-MFI and H-FAU zeolites.[18]

Another parallel catalytic cycle (*Cycle 3*, Scheme 2) converts the alkanal to *n*-diene via the decomposition of an adsorbed alkanal−alkenol pair (AAP*) into a protonated alkanal (A*) and an allylic alcohol (Step R3.1a), followed by the dehydration of the allylic alcohol (Step R3.2a) to evolve a diene, as shown in Scheme 3. The relative rates for isomerization and dehydration are probed by comparing the rates of butadiene formation from butanal ($r_{\mathrm{Dehy,butanal}}$) and those of crotyl alcohol dehydration ($r_{\mathrm{Dehy,crotyl\ alcohol}}$) on $H_4SiW_{12}O_{40}$ clusters at 573 K. The butadiene formation rates are significantly smaller (by 118 times) than those of crotyl alcohol dehydration ($r_{\mathrm{Dehy,butanal}}$ = 0.38 ± 0.06 mmol $(\mathrm{mol_{H^+}}\ \mathrm{s})^{-1}$ vs $r_{\mathrm{Dehy,crotyl\ alcohol}}$ = 45 mmol $(\mathrm{mol_{H^+}}\ \mathrm{s})^{-1}$, 573 K, space velocity of 0.045 mol reactant $(\mathrm{mol_{H^+}}\ \mathrm{s})^{-1}$); thus, the initial isomerization step (Step R3.1a) must be kinetically relevant. It is expected that this kinetically relevant allylic alcohol formation step could also take place on a protonated alkanal monomer (A*) (Step R3.1b). The proposed mechanism leads to the rate equations for diene formation via bimolecular (*Cycle 3*, $r_{\mathrm{Dehy,bi}}$) and monomolecular (*Cycle 3.1*, $r_{\mathrm{Dehy,mono}}$) pathways, respectively:

$$r_{\mathrm{Dehy,bi}} = \frac{k_{\mathrm{iso,bi}}\dfrac{k_{\mathrm{AAP}}(K_{\mathrm{ads}}[\mathrm{H^+}]P_{\mathrm{alkanal}})\cdot(K_{\mathrm{taut}}P_{\mathrm{alkanal}})}{k_{-\mathrm{AAP}}+k_{\mathrm{C-C}}+k_{\mathrm{iso,bi}}}}{\underset{(\mathrm{H^+site})}{[\mathrm{H^+}]} + \underset{(\mathrm{A^*})}{K_{\mathrm{ads}}[\mathrm{H^+}]P_{\mathrm{alkanal}}} + \underset{(\mathrm{AAP^*})}{\dfrac{k_{\mathrm{AAP}}(K_{\mathrm{ads}}[\mathrm{H^+}]P_{\mathrm{alkanal}})(K_{\mathrm{taut}}P_{\mathrm{alkanal}})}{k_{-\mathrm{AAP}}+k_{\mathrm{C-C}}+k_{\mathrm{iso,bi}}}} + \underset{(\mathrm{other})}{\alpha}} \tag{9}$$

$$r_{\mathrm{Dehy,mono}} = \frac{k_{\mathrm{iso,mono}}K_{\mathrm{ads}}[\mathrm{H^+}]P_{\mathrm{alkanal}}}{\underset{(\mathrm{H^+site})}{[\mathrm{H^+}]} + \underset{(\mathrm{A^*})}{K_{\mathrm{ads}}[\mathrm{H^+}]P_{\mathrm{alkanal}}} + \underset{(\mathrm{AAP^*})}{\dfrac{k_{\mathrm{AAP}}(K_{\mathrm{ads}}[\mathrm{H^+}]P_{\mathrm{alkanal}})(K_{\mathrm{taut}}P_{\mathrm{alkanal}})}{k_{-\mathrm{AAP}}+k_{\mathrm{C-C}}+k_{\mathrm{iso,bi}}}} + \underset{(\mathrm{other})}{\alpha}} \tag{10}$$

where $k_{\mathrm{iso,bi}}$ and $k_{\mathrm{iso,mono}}$ are the rate constants for alkanal isomerization via bimolecular (Step R3.1a) and monomolecular (Step R3.1b) pathways, respectively. All the other rate and equilibrium constants are defined above and in Scheme 3 and the denominator terms remain identical with those in eqs 4 and 6. Equations 9 and 10 simplify to the following, when protonated alkanal (A*) is the most abundant surface intermediate:

$$r_{\mathrm{Dehy,bi}} = \frac{k_{\mathrm{iso,bi}}k_{\mathrm{AAP}}K_{\mathrm{taut}}}{k_{-\mathrm{AAP}} + k_{\mathrm{C-C}} + k_{\mathrm{iso,bi}}}P_{\mathrm{alkanal}} = k_{\mathrm{Dehy,bi,eff}}P_{\mathrm{alkanal}} \tag{11a}$$

$$k_{\mathrm{Dehy,bi,eff}} = \frac{k_{\mathrm{iso,bi}}k_{\mathrm{AAP}}K_{\mathrm{taut}}}{k_{-\mathrm{AAP}} + k_{\mathrm{C-C}} + k_{\mathrm{iso,bi}}} \tag{11b}$$

$$r_{\mathrm{Dehy,mono}} = k_{\mathrm{iso,mono}} = k_{\mathrm{Dehy,mono,eff}}P_{\mathrm{alkanal}}{}^{0} \tag{12a}$$

$$k_{\mathrm{Dehy,mono,eff}} = k_{\mathrm{iso,mono}} \tag{12b}$$

Equations 11a and 12a show that $r_{\mathrm{Dehy,bi}}$ increases proportionally with alkanal pressure (P_{alkanal}) whereas $r_{\mathrm{Dehy,mono}}$ remains insensitive to alkanal pressure. The terms $k_{\mathrm{iso,bi}}k_{\mathrm{AAP}}K_{\mathrm{taut}}(k_{-\mathrm{AAP}} + k_{\mathrm{C-C}} + k_{\mathrm{iso,bi}})^{-1}$ and $k_{\mathrm{iso,mono}}$ are the effective rate constants for bimolecular and monomolecular pathways for alkanal dehydration ($k_{\mathrm{Dehy,bi,\ eff}}$ and $k_{\mathrm{Dehy,mono,\ eff}}$), respectively, as shown in eqs 11b and 12b. The sum of these rates from the two pathways gives the overall rate of diene formation, r_{Dehy}:

$$\begin{aligned} r_{\mathrm{Dehy}} &= r_{\mathrm{Dehy,bi}} + r_{\mathrm{Dehy,mono}} \\ &= k_{\mathrm{Dehy,bi,eff}}P_{\mathrm{alkanal}} + k_{\mathrm{Dehy,mono,eff}} \end{aligned} \tag{13}$$

In the proposed mechanism (Scheme 3), alkanal isomerization (Steps R3.1a and R3.1b) requires participation of a vicinal lattice oxygen (basic site) adjacent to the H^+ site as a hydrogen abstractor to promote the double bond shift from a C═O bond to a C═C bond.[17] The rate of isomerization is expected to depend on the number of these H^+ and lattice oxygen pairs that function together as the acid−base site pairs. The catalytic involvement of an acid−base site pair in alkanal isomerization was also found on H-ZSM-5 zeolite: the removal of extraframework Al_2O_3 (by ∼65%) from H-ZSM-5 via $(NH_4)_2SiF_6$ treatment suppresses the rate of isomerization−dehydration commensurately by about half without affecting those of intermolecular and intramolecular C═C bond formation (see Table S2 and Figure S4 in Section S4 of the Supporting Information). This confirms that a portion of the isomerization−dehydration turnovers requires extraframework Al_2O_3, which contains a bridging oxygen ion between two Al ions,[34] acting cooperatively with an adjacent H^+ site as an acid−base site pair in the isomerization step. On the Keggin anion ($SiW_{12}O_{40}{}^{4-}$), all the lattice oxygen atoms on the external surface, which include 12 terminal oxygens (W═O) and 24 bridging oxygens (W−O−W), can act as the conjugated base sites for the protons (H^+).[22] Because each terminal oxygen has four and each bridging oxygen has six adjacent surface oxygen sites, alkanal molecules can easily find the acid−base site pairs to undergo isomerization−dehydration on $H_4SiW_{12}O_{40}$ clusters. In the contrasting case of MFI zeolites, only the O atoms of the framework AlO_4 tetrahedrons can act as the conjugated base sites. Typically three out of the four O atoms in AlO_4 tetrahedrons are exposed in the zeolite channels and remained accessible to the reactant. A small amount of extraframework Al−O−Al structures may be located next to the H^+ sites, in which case the extraframework O and the H^+ sites form an acid−base site pair. Generally, the H^+ sites in zeolites have much fewer adjacent base sites in comparison to those on $H_4SiW_{12}O_{40}$ clusters. As a result, alkanal molecules have a smaller chance to encounter acid−base site pairs and thus a lower rate for isomerization−dehydration on zeolites than on $H_4SiW_{12}O_{40}$ (e.g., r_{Dehy} = 1.3 vs 0.19 mmol $(\mathrm{mol_{H^+}}\ \mathrm{s})^{-1}$ on $H_4SiW_{12}O_{40}$ and H-MFI, respectively, time on stream 35 min, 573 K, 1.1 kPa butanal, as shown in Figure 5 and Figure S2c in the Supporting Information, respectively).

As the reaction time increased, the rate for alkanal dehydration (r_{Dehy}) gradually decreased: from 1.3 mmol

Scheme 4. Proposed Mechanism for (a) Acid-Catalyzed Cyclization−Dehydration of 2,4-Heptadienal ($C_7H_{10}O$)[a] and (b) Acid-Catalyzed Cyclization−Dehydration of 2,4-Diethyl-2,4-octadienal ($C_{12}H_{20}O$) during Butanal Reactions[b]

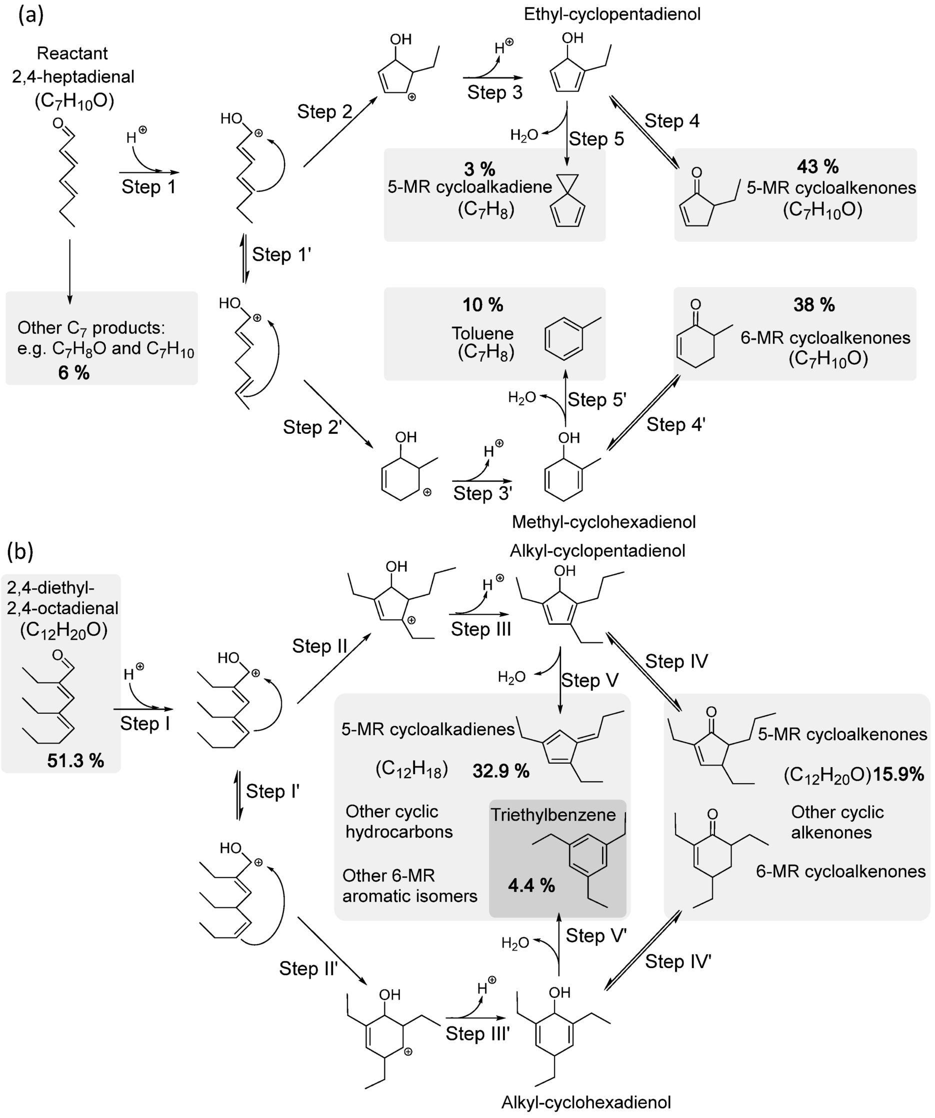

[a] The products detected are labeled with carbon selectivities within the C_7 product fractions during 2,4-heptadienal reactions on $H_4SiW_{12}O_{40}$ at 573 K, 2,4-heptadienal pressure 0.2 kPa, space velocity 0.009 mol $(\text{mol}_{H^+}\ s)^{-1}$, and time on stream 125 min. [b] The products detected are labeled with carbon selectivities within the C_{12} product fractions during butanal reaction on $H_4SiW_{12}O_{40}$ at 573 K, butanal pressure 1.1 kPa, space velocity 0.045 mol $(\text{mol}_{H^+}\ s)^{-1}$, and time on stream 125 min.

$(\text{mol}_{H^+}\ s)^{-1}$ at 35 min to 0.44 mmol $(\text{mol}_{H^+}\ s)^{-1}$ at 155 min (Figure 5), although the number of H^+ sites remained relatively stable during this period (>30 min, Figure 1b). We surmise that, as the reaction time increases, the deposition of heavy products (e.g., aromatics and cokes) may poison the lattice oxygen (basic sites), making a large portion of the acid−base site pairs inaccessible to alkanals, thus leading to a decrease in $k_{\text{iso,bi}}$ and $k_{\text{iso,mono}}$ and in turn the isomerization rates (eqs 11a and 12a).

As $k_{\text{iso,bi}}$ decreases, the rate of AAP* consumption by Step R3.1a decreases and, as a result, the coverage of AAP* intermediates (Scheme 3) increases concomitantly. This trend between $k_{\text{iso,bi}}$ and the coverage of the AAP* intermediate is captured by the term $k_{\text{AAP}}(K_{\text{ads}}[H^+]P_{\text{alkanal}})(K_{\text{taut}}P_{\text{alkanal}})(k_{-\text{AAP}} + k_{\text{C−C}} + k_{\text{iso, bi}})^{-1}$ in the denominator of eq 4. Such changes led to an increase in the effective rate constant $k_{\text{Inter,eff}}$ and the rate r_{Inter} for intermolecular C=C bond formation (*Cycle 1*, Scheme 2) with reaction time, according to eqs 5b and 5a, as shown in Figure 5. After 155 min of reaction, the changes in r_{Inter} and r_{Dehy} values became much slower than those during the initial times: the changes in rate value with time, $\Delta r_{\text{Inter}}(\Delta\text{time-on-stream})^{-1}$ and $\Delta r_{\text{Dehy}}(\Delta\text{time-on-stream})^{-1}$, were 1 order of magnitude smaller at 155 min than at 35 min (Figure 5). At these longer reaction times, most of the basic sites were deactivated by coke deposition and the number of acid and basic sites remained essentially constant. Thus, $k_{\text{iso,bi}}$ and $k_{\text{iso,mono}}$ and the effective rate constants ($k_{\text{Dehy,bi,eff}}$ and $k_{\text{Dehy,mono,eff}}$) remained constant. The rate data in Figure 4c reflect the overall rates of diene formation, r_{Dehy}, at these longer reaction times. The slopes in Figure 4c are related to the effective rate constants for the bimolecular pathway ($k_{\text{Dehy,bi,eff}}$) while the intercepts reflect the effective rate constants for the monomolecular pathway ($k_{\text{Dehy,mono,eff}}$) for diene formation.

3.4. Catalytic Sequences for Secondary Cyclization−Dehydration That Form Aromatics and Cycloalkadienes on $H_4SiW_{12}O_{40}$ Clusters. In this section, we describe the secondary cyclization−dehydration reactions (*Cyclization 1, Cyclization 2, Cyclization 2.1,* and *Cyclization 3* in Scheme 2) that form cycloalkadienes ($C_{tn}H_{2tn-2t}$, $n = 3-6$, $t = 2$) and aromatics ($C_{tn}H_{2tn-2t}$, $n = 3-6$, $t = 3-4$, including alkyl benzenes ($t = 3$) and alkyl tetralins ($t = 4$)), as shown in Scheme 2. These secondary, larger products all contain carbon numbers equal to multiples (t) of the parental alkanal unit (C_n), as shown from the carbon distributions in Figure 3, because they are products of the stepwise alkanal addition reactions. In each of these steps, an alkanal unit was added to the carbon chain in an intermolecular carbon−carbon bond formation event. The carbon chain growth is consistent with the increase in the carbon selectivities toward larger alkenals ($C_{12}H_{20}O$ and $C_{16}H_{26}O$) and hydrocarbons (including C_8 cycloalkadienes, C_{12} and C_{16} aromatics) as the space velocity decreases during butanal (C_4H_8O) reactions at 623 K (Figure 2a). As shown in Scheme 1, the larger C_{tn} alkenal products ($C_{tn}H_{2tn-2t+2}O$, $n = 3-6$, $t = 2-4$) may further undergo cyclization to form C_{tn} cycloalkenols or cycloalkadienols ($C_{tn}H_{2tn-2t+2}O$, $n = 3-6$, $t = 2-4$) (Steps 2b and 3b), before their dehydration to produce C_{tn} cycloalkadienes ($C_{tn}H_{2tn-2t}$, $n = 3-6$, $t = 2$) or aromatics ($C_{tn}H_{2tn-2t}$, $n = 3-6$, $t = 3-4$) (Steps 2d and 3d), as also captured in eq 14:

$$\underset{\text{alkenal}}{C_{tn}H_{2tn-2t+2}O} \xrightarrow{\text{cyclization}} \underset{\text{cycloalkenol or cycloalkadienol}}{C_{tn}H_{2tn-2t+2}O} \xrightarrow{\text{dehydration}} \underset{\text{aromatic or cyclodiene}}{C_{tn}H_{2tn-2t}} + H_2O \qquad (14)$$

These aromatic or cycloalkadiene species ($C_{tn}H_{2tn-2t}$) (*Cyclizations 1, 2, 2.1,* and 3 in Scheme 2) can act as hydrogen donors (denoted as $R'H_2$ in eq 2a and Scheme 3) for the intramolecular C═C bond formation (*Cycle 2*, Scheme 2), as discussed in sections 3.2 and 3.3. These H donors may also donate their hydrogen atoms to protonated alkenals ($C_{tn}H_{2tn-2t+2}OH^+$, $n = 3-5$, $t = 2-4$), possibly through the hydride transfer steps described in section 3.2, forming $C_{tn}H_{2tn-2t+2}$ instead of $C_{tn}H_{2tn-2t}$ ($n = 3-6$, $t = 2-4$). This route, however, is a minor pathway with the carbon selectivities, defined as $C_{tn}H_{2tn-2t+2}$ $(C_{tn}H_{2tn-2t+2} + C_{tn}H_{2tn-2t})^{-1}$, smaller than 15% and thus will not be addressed here.

Cyclization of long-chain (carbon number >5) alkenals such as citral,[35−39] citronellal,[38,40] and aromatic aldehydes (e.g., β-styrylacetaldehyde)[41−44] catalyzed by hydronium ions derived from HCl and H_2SO_4 has been studied extensively in the aqueous phase. The reaction is initiated by protonation of their carbonyl group, followed by an intramolecular electrophilic attack of the positively charged carbonyl carbon to the C═C double bond, creating an intramolecular C−C bond and a hydroxyl group and forming cycloalkenol as the product.[37,38] Sequential dehydration of the cycloalkenol removes the hydroxyl group and creates the C═C bond, leading to the formation of a stable aromatic ring. The cycloalkenol can also rearrange via a parallel reaction that forms cycloketone through keto−enol tautomerization. We hypothesize that the cyclization of larger alkenal products in alkanal reactions (e.g., 2,4-diethyl-2,4-octadienal from butanal reactions) occurs via a mechanism similar to those of citral and citronellal.[37,38] We probe this reaction using 2,4-heptadienal ($C_7H_{10}O$), because its structure and functional groups resemble those of 2,4-diethyl-2,4-octadienal produced from intermolecular C═C bond formation between butanal and 2-ethyl-2-hexenal (Step 3a, Scheme 1).

The reactions of 2,4-heptadienal ($C_7H_{10}O$) on $H_4SiW_{12}O_{40}$ clusters (573 K) led predominantly to $C_{14}H_{18}O$ (alkenals and isomers), $C_7H_{10}O$ (alkyl cycloalkenones), and C_7H_8 (toluene and a five-membered-ring cycloalkadiene), with carbon selectivities of 63.4, 29.3, and 4.8%, respectively (Figure S6 in the Supporting Information). These product distributions suggest that 2,4-heptadienal ($C_7H_{10}O$) reactions occur via two major pathways: (i) intermolecular C═C bond formation between two $C_7H_{10}O$ reactants, producing larger $C_{14}H_{18}O$ alkenals and (ii) cyclization−dehydration leading to the formation of cycloalkenones and cyclic hydrocarbon species. Scheme 4a shows the proposed mechanism for 2,4-heptadienal cyclization−dehydration, similar to that for citral and citronellal.[37,38] The cyclization is initiated by the protonation of 2,4-heptadienal (Step 1, Scheme 4) and the following intramolecular C−C bond coupling (Step 2) and deprotonation (Step 3) that lead to a five-membered-ring (5-MR) alkyl cyclopentadienol. The cyclopentadienol can either isomerize to form the more stable 5-MR cycloalkenone isomers (Step 4, carbon selectivity 43% within all C_7 products) or dehydrate to evolve a 5-MR cycloalkadiene (Step 5, carbon selectivity 3%). The protonated 2,4-heptadienal could undergo C═C bond shift (Step 1′) followed by cyclization to form a six-membered-ring (6-MR) cyclohexadienol (Steps 2′ and 3′), and this route would lead to the formation of 6-MR cycloalkenones (Step 4′, carbon selectivity 38%) and aromatic product, toluene (Step 5′, carbon selectivity 10%).

For the secondary cyclization−dehydration of 2,4-diethyl-2,4-octadienal ($C_{12}H_{20}O$) during butanal reactions, we could only determine the chemical formulas but not the detailed chemical structures for most of the products by mass spectrometry. Nevertheless, it is plausible to propose a cyclization−dehydration mechanism on the basis of the study using 2,4-heptadienal ($C_7H_{10}O$) in Scheme 4a. Scheme 4b shows the proposed cyclization−dehydration pathways for 2,4-diethyl-2,4-octadienal ($C_{12}H_{20}O$). The cyclization reactions involve carbonyl protonation (Step I), C═C bond shift (Step I′), intramolecular C−C bond coupling (Step II or II′), and deprotonation (Step III or III′), evolving 5-MR or 6-MR alkyl cycloalkadienols. These cycloalkadienols can undergo either isomerization (Step IV or IV′) to form 5-MR or 6-MR cycloalkenone isomers ($C_{12}H_{20}O$, carbon selectivity 15.9% within all C_{12} products) or dehydration (Step V or V′) to evolve 5-MR or 6-MR cycloalkadienes ($C_{12}H_{18}$, carbon selectivity 32.9% within all C_{12} products). It was noted that the branched structure of 2,4-diethyl-2,4-octadienal resulted in diverse cyclization−dehydration products due to the concomitant isomerization reactions. In fact, there were more than 20 different types of $C_{12}H_{18}$ products being detected with the highest selectivities (4.4%, within all C_{12} products) toward 1,3,5-triethylbenzene.

These results led to the proposed pathway for alkanal chain growth in Scheme 1. Larger alkenals ($C_{tn}H_{2tn-2t+2}O$, $n = 3-6$, $t = 2, 3$) produced from the sequential, intermolecular C═C bond formation steps (Steps 2a and 3a) undergo cyclization (Steps 2b and 3b) and evolve cycloalkenols/cycloalkadienols ($C_{tn}H_{2tn-2t+2}O$, $n = 3-6$, $t = 2, 3$). The cycloalkenols/cycloalkadienols can either rearrange and desorb as cycloalkanones/cycloalkenones (Steps 2c and 3c) or dehydrate (Steps 2d and 3d) to evolve unsaturated hydrocarbon species

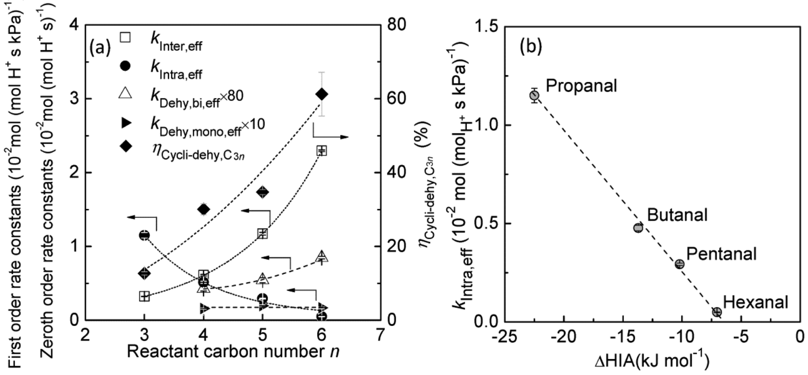

Figure 6. (a) Rate constants for intermolecular C═C bond formation ($k_{\text{Inter,eff}}$, □, *Cycle 1* in Scheme 2), intramolecular C═C bond formation ($k_{\text{Intra,eff}}$, ●, *Cycle 2*), and alkanal isomerization−dehydration via bimolecular pathway ($k_{\text{Dehy,bi,eff}}$, △, *Cycle 3*) and monomolecular pathway ($k_{\text{Dehy,mono,eff}}$, ▶, *Cycle 3.1*), and cyclization−dehydration selectivity of C_{3n} alkenal ($\eta_{\text{Cycli-dehy,C}_{3n}}$, ◆, *Cyclizations 2* and *2.1* in Scheme 2, eq 15) during alkanal ($C_nH_{2n}O$, $n = 3-6$) deoxygenation on $H_4SiW_{12}O_{40}$ clusters at 573 K as a function of reactant carbon number ($C_nH_{2n}O$ 1.1−10 kPa, 0.045−0.44 $\text{mol}_{\text{alkanal}}$ $(\text{mol}_{\text{H}^+}\ \text{s})^{-1}$, alkanal conversion 14−17, 26-31, 45−47, and 68−72% for propanal, butanal, pentanal, and hexanal, respectively). (b) First-order rate constants for intramolecular C═C bond formation ($k_{\text{Intra,eff}}$) for C_3−C_6 alkanals ($C_nH_{2n}O$, $n = 3-6$) on $H_4SiW_{12}O_{40}$ clusters at 573 K as a function of the hydride ion affinity difference (ΔHIA) between the carbenium ions of H donor ($R'H^+$) and the protonated alkanal ($C_nH_{2n}OH^+$) ($\Delta\text{HIA} = \text{HIA}_{R'H^+} - \text{HIA}_{C_nH_{2n}OH^+}$, where $R'H^+ = C_{10}H_{11}{}^+$, as tetralin ($C_{10}H_{12}$) is used as the representative H donor to estimate ΔHIA values).

(including cycloalkadienes and aromatics, $C_{tn}H_{2tn-2t}$, $n = 3-6$, $t = 2, 3$). These pathways led almost exclusively to hydrocarbons with defined carbon numbers tn, as shown in Figure 3, because transalkylation reactions of the aromatic products, which shift the methyl or ethyl groups among the aromatics, remained kinetically insignificant. As an example, reactions of butanal (C_4H_8O) on $H_4SiW_{12}O_{40}$ clusters at 573 K produced almost exclusively cycloalkadienes or aromatics with 8, 12, or 16 carbon atoms (carbon selectivities >99%, Figure 3b). In contrast, the same reactions on H-form zeolites (H-ZSM-5[11,18] and H-Y[18]) produced aromatic products with diverse carbon numbers ranging from C_6 to C_{16+}. The distinct carbon distributions between the $H_4SiW_{12}O_{40}$ clusters and microporous crystalline materials were caused by effective transalkylation reactions inside the pores and cages of zeolites, which did not occur on $H_4SiW_{12}O_{40}$ clusters.

Previous studies have shown that Keggin polyoxometalate clusters ($H_3PW_{12}O_{40}$ and $H_4SiW_{12}O_{40}$), either dispersed on SiO_2[45] or supported on the external surfaces of dealuminated zeolite Y,[46] could catalyze the transalkylation of alkyl benzenes (trimethylbenzene and toluene), leading to C_6−C_{10+} aromatics at moderate temperatures (573−723 K). Reactions of tetralin ($C_{10}H_{12}$) in the absence of alkanals could provide the reactivities of aromatic transalkylation. In the absence of an alkanal, tetralin reactions on $H_4SiW_{12}O_{40}$ formed not only C_{10} naphthalene as the dehydrogenation product but also C_6−C_{13} aromatics via transalkylation reactions. The carbon selectivity toward the transalkylation products ($1 - C_{10}/\sum_{m=6}^{m=13}C_m$) was 7.2% and the transalkylation rate was 0.40 mmol tetralin $(\text{mol}_{\text{H}^+}\ \text{s})^{-1}$ at 573 K (space velocity 5.6 $\text{mmol}_{\text{tetralin}}$ $(\text{mol}_{\text{H}^+}\ \text{s})^{-1}$). These selectivity values were similar to those of tetralin reactions on H-Y zeolite (Si/Al = 15), where the transalkylation selectivity ($1 - C_{10}/\sum_{m=6}^{m=13}C_m$) was 20% and transalkylation rate was 0.11 $\text{mmol}_{\text{tetralin}}$ $(\text{mol}_{\text{H}^+}\ \text{s})^{-1}$ at 573 K (space velocity 0.57 $\text{mmol}_{\text{tetralin}}$ $(\text{mol}_{\text{H}^+}\ \text{s})^{-1}$). These selectivities contradicted those on $H_4SiW_{12}O_{40}$ clusters after butanal catalysis at 573 K for >155 min, which showed no transalkylation reactivity of tetralin at 573 K. These results, together with the lack of transalkylation of aromatic products (C_8, C_{12}, and C_{16}) detected during butanal reactions at 573 K (Figure 3b), indicate that butanal adsorption inhibits the transalkylation activity on $H_4SiW_{12}O_{40}$ clusters. The lack of detectable transalkylation reactivities during alkanal reactions on $H_4SiW_{12}O_{40}$ is likely caused by the loss of strong H^+ sites resulting from their binding to heavier products (e.g., cokes), as confirmed from temperature-programmed desorption of pyridine carried out on $H_4SiW_{12}O_{40}$ clusters after steady-state reactions (see Figure S5 in the Supporting Information). Similar conclusions have also been shown previously for transalkylation of alkyl aromatics on a series of HNa-Y and H-USY zeolites, which indicated that only strong Brønsted acid sites with NH_3 desorption temperatures above 623 K were active in transalkylation reactions.[47]

3.5. Effects of Alkanal Chain Length on Its Deoxygenation Rates and Selectivities on $H_4SiW_{12}O_{40}$ Clusters.

Figure 6a shows the rate constants ($k_{\text{Inter,eff}}$, $k_{\text{Intra,eff}}$, $k_{\text{Dehy,bi,eff}}$, and $k_{\text{Dehy,mono,eff}}$ in eqs 5, 8, 11, and 12, respectively) for the primary pathways (*Cycles 1*, *2*, *3*, and *3.1*, in Scheme 2) of C_3−C_6 n-alkanal reactions on $H_4SiW_{12}O_{40}$ at 573 K and the selectivities for secondary cyclization−dehydration reactions (*Cyclization 2*, Scheme 2), $\eta_{\text{Cycli-dehy,C}_{3n}}$, defined as the site time yield of C_{3n} aromatics ($r_{C_{3n}\ \text{arom}}$) divided by that of all C_{3n} products, including oxygenates and aromatics ($r_{C_{3n}\ \text{overall}}$):

$$\eta_{\text{Cycli-dehy,C}_{3n}} = \frac{r_{C_{3n}\text{arom}}}{r_{C_{3n}\text{overall}}} \tag{15}$$

Next, we decompose the effective rate constants ($k_{\text{Inter,eff}}$, $k_{\text{Intra,eff}}$, $k_{\text{Dehy,bi,eff}}$, and $k_{\text{Dehy,mono,eff}}$) to elementary rate and equilibrium constants and connect these reactivity trends to the thermodynamic properties of Brønsted site and reactants. According to eqs 5 and 11, the effective rate constant ratio for intermolecular C═C bond formation ($k_{\text{Inter,eff}}$) to isomerization−dehydration ($k_{\text{Dehy,bi,eff}}$) equals the rate constant ratio for aldol condensation ($k_{\text{C−C}}$, Step R1.2) to alkanal isomerization ($k_{\text{iso,bi}}$, Step R3.1a):

$$\frac{k_{\text{Inter,eff}}}{k_{\text{Dehy,bi,eff}}} = \frac{k_{\text{C}-\text{C}}}{k_{\text{iso,bi}}} \tag{16}$$

As shown in Figure 6a, during steady-state reaction, $k_{\text{Inter,eff}}$ is much higher than $k_{\text{Dehy,bi,eff}}$ with $k_{\text{Inter,eff}}$ $(k_{\text{Dehy,bi, eff}})^{-1}$ ratios of 114, 173, and 217 for butanal, pentanal, and hexanal, respectively; thus, $k_{\text{C}-\text{C}}$ is much larger than $k_{\text{iso,bi}}$. Therefore, the effective rate constants for the intermolecular C═C formation (eq 5) and the alkanal dehydration via bimolecular pathway (eq 11) can be simplified further to

$$k_{\text{Inter,eff}} = \frac{k_{\text{C}-\text{C}} k_{\text{AAP}} K_{\text{taut}}}{k_{-\text{AAP}} + k_{\text{C}-\text{C}}} \tag{17}$$

$$k_{\text{Dehy,bi,eff}} = \frac{k_{\text{iso,bi}} k_{\text{AAP}} K_{\text{taut}}}{k_{-\text{AAP}} + k_{\text{C}-\text{C}}} \tag{18}$$

Equation 17 indicates that $k_{\text{Inter,eff}}$ depends on the rate constants for alkanal−alkenol pair (AAP*) formation (k_{AAP}, Step R1.1), its reverse reaction ($k_{-\text{AAP}}$, Step R1.1′), and aldol condensation ($k_{\text{C}-\text{C}}$, Step R1.2), as well as on the equilibrium constant for keto−enol tautomerization (K_{taut}, Step G1).

As the alkanal reactant size increases from C_3 to C_6, the effective rate constant $k_{\text{Inter,eff}}$ increases (as shown in Figure 6a), reflecting the increase in the values of k_{AAP}, $k_{\text{C}-\text{C}}$, and/or K_{taut}. Little information on K_{taut} values is available for the keto−enol tautomerization of gaseous C_3−C_6 *n*-alkanals. However, it is known that the equilibrium constant for keto−enol tautomerization (K_{taut}) of isobutyraldehyde in the aqueous phase is much higher than that of acetaldehyde (1.28×10^{-4} vs 5.89×10^{-7}, at 298 K),[48−50] which suggests that a larger alkyl substituent favors the enol formation and thus exhibits higher K_{taut} values. This is because the $\sigma-\pi$ hyperconjugation between the alkyl substituent and the enol C═C bond delocalizes electrons of the alkyl group onto the C═C bond and stabilizes the enol;[48,51,52] larger alkyl substituents promote the enol stabilization to a greater extent.

We expect that the larger alkanals favor the formation of the adsorbed alkanal−alkenol pair (AAP*, Step R1.1) and the bimolecular transition state for aldol condensation (TS(C−C)*, Step R1.2) on $H_4SiW_{12}O_{40}$ clusters, because of their stronger van der Waals interactions with the catalyst surfaces.[53] As an example, van der Waals interactions increase with the carbon number in *n*-alkanes, causing the heats of *n*-alkane adsorption to increase by 1.5−2 kJ mol^{-1} for each additional C atom, when they are adsorbed on mesoporous silica structures.[54] Therefore, we expect the larger alkanal to exhibit a higher rate constant for AAP* formation (k_{AAP}, Step R1.1). In the aldol condensation step (Step R1.2), both the reactant state (AAP*) and transition state (TS(C−C)*) contain the same carbon number and therefore the extent of stabilization remains the same. For this reason, we expect that the activation barrier for TS(C−C)* formation and the related $k_{\text{C}-\text{C}}$ remain insensitive to the alkanal reactant size. Thus, the higher effective rate constants $k_{\text{Inter,eff}}$ for larger alkanals must reflect their higher K_{taut} and k_{AAP} values, which correspond to the higher stability of enol tautomer and more abundant AAP* intermediates, respectively, in comparison to the smaller alkanals.

The effective rate constants for alkanal dehydration via the monomolecular pathway (Steps R3.1b and R3.2b), $k_{\text{Dehy,mono,eff}}$, remain relatively stable for C_4−C_6 alkanals, as shown in Figure 6a; thus, the alkanal isomerization step ($k_{\text{iso,mono}}$, Step R3.1b) is not sensitive to the alkanal reactant size. It is plausible that the rate constant for alkanal isomerization via the bimolecular pathway ($k_{\text{iso,bi}}$, Step R3.1a) is also not sensitive to the reactant size. As a result, the larger alkanals with higher k_{taut} and k_{AAP} values exhibit a higher effective rate constant $k_{\text{Dehy,bi, eff}}$ according to eq 18, as shown in Figure 6a.

In contrast to the rate constant trends for the intermolecular C═C bond formation and isomerization−dehydration reactions ($k_{\text{Inter,eff}}$ and $k_{\text{Dehy,bi,eff}}$), the effective rate constant for intramolecular C═C bond formation ($k_{\text{Inter,eff}}$) decreases with increasing alkanal carbon number. As shown in eqs 7 and 8, the effective rate constant $k_{\text{Inter,eff}}$ reflects the elementary rate constant for the hydride transfer step (k_{HT}, Step R2.1, Scheme 3). During the hydride transfer, H donors ($R'H_2$) donate their hydride ions to protonated alkanals ($C_nH_{2n}OH^+$) and convert into carbenium ions ($R'H^+$) (Step R2.2), because $C_nH_{2n}OH^+$ has a higher hydride ion affinity (HIA) than $R'H^+$. The hydride ion affinity difference (ΔHIA) between the carbenium ion of the H donor ($R'H^+$, $\text{HIA}_{R'H^+}$) and the protonated alkanal as the H acceptor ($C_nH_{2n}OH^+$, $\text{HIA}_{C_nH_{2n}OH^+}$) dictates the hydride transfer reactivity:

$$\Delta\text{HIA} = \text{HIA}_{R'H^+} - \text{HIA}_{C_nH_{2n}OH^+} \tag{19}$$

The H-donor−H-acceptor pairs with more negative ΔHIA values exhibited higher hydride transfer rates. Because the alkyl tetralins in the aromatic product fractions are the major H donors for alkanal transfer hydrogenation,[18] we use tetralin ($C_{10}H_{12}$) as the representative H donor ($R'H^+ = C_{10}H_{11}{}^+$, $\text{HIA}_{R'H^+} = 934.1$ kJ mol^{-1}[18]) to estimate the ΔHIA values for different alkanals. As the carbon number (*n*) of alkanal increased from 3 to 6, its $\text{HIA}_{C_nH_{2n}OH^+}$ value decreased from 956.6 to 941.1 kJ mol^{-1} and the ΔHIA increased from −22.5 to −7.0 kJ mol^{-1}. The less negative ΔHIA values led the $k_{\text{Intra,eff}}$ value to concomitantly decrease from 11.5 to 0.48 mmol $(\text{mol}_{H^+}\ \text{s kPa})^{-1}$ (573 K, Figure 6b). This direct correlation between the reactivities and the ΔHIA has also been demonstrated previously on H-FAU zeolites.[18]

The reactivity of the secondary cyclization−dehydration reactions also increased with the alkanal size, as indicated by the higher molar percentages of C_{2n} cycloalkadienes and C_{3n} aromatics in the C_{2n} and C_{3n} product fractions (Figure 3) and higher cyclization−dehydration selectivities toward C_{3n} alkenal ($\eta_{\text{Cycli-dehy},C_{3n}}$, eq 15, Figure 6a) for the larger alkanals. The cyclization−dehydration pathway requires the electrophilic attack of the carbonyl carbon onto the C═C double bond, a step promoted by an alkyl substitution at the C═C position, because the substitution leads to higher electron densities at the C═C bond.[42] As the chain length of the alkanal increases, the larger alkyl group at the C═C position (−R group, as shown in Scheme 1) affords more effective electron donation and thus results in larger cyclization−dehydration rates.

4. CONCLUSIONS

Kinetic measurements and acid site titration lead to a proposed reaction network with parallel and sequential catalytic cycles for the deoxygenation of light alkanals ($C_nH_{2n}O$, $n = 3$−6) catalyzed by the Brønsted acid sites (H^+) on tungstosilicic acid clusters ($H_4SiW_{12}O_{40}$). Alkanal deoxygenation proceeds via three primary pathways: (1) intermolecular C═C bond formation, which couples two alkanal molecules via a kinetically relevant aldol-condensation step followed by a rapid dehydration step, which evolves a larger alkenal ($C_{2n}H_{4n-2}O$),

(2) intramolecular C═C bond formation, which converts alkanals directly to *n*-alkenes (C_nH_{2n}), via kinetically relevant hydride ion transfer from H-donating agents to protonated alkanals, followed by dehydration, and (3) isomerization−dehydration, during which the alkanals first isomerize to form allylic alcohols then rapidly dehydrate to produce *n*-dienes (C_nH_{2n-2}). In the catalytic cycle of pathway 1, a series of sequential intermolecular C═C bond formation events adds additional alkanal units onto the carbon chain, thus producing larger alkenals ($C_{3n}H_{6n-4}O$ and $C_{4n}H_{8n-6}O$). These larger alkenal species can undergo cyclization−dehydration reactions, leading to cyclic hydrocarbons including cycloalkadiene ($C_{2n}H_{4n-4}$) and aromatic species ($C_{3n}H_{6n-6}$ or $C_{4n}H_{8n-8}$). The catalytic pathways are kinetically coupled together, because cyclic hydrocarbons produced from the sequential reactions of pathway 1 act as the hydrogen donors for pathway 2 and pathways 1 and 3 share the coadsorbed alkanal−alkenol pairs as the common reaction intermediates.

The molecular size of alkanals affects their thermochemical properties and in turn influences the stabilities of the transition states and reaction intermediates in the kinetically relevant steps of the different pathways. These effects lead to contrasting reactivity trends for the various reaction pathways, thus resulting in different selectivities across the alkanal family. The rate constants for pathway 1 and for the bimolecular route of pathway 3 both increase with alkanal size, apparently because both reactions require enol tautomers, which are more stable for larger alkanals, for the formation of bimolecular alkanal−alkenol pairs as the reaction intermediates. Alkanal size does not affect the rate constants for the monomolecular route of pathway 3, because protonated alkanal monomers remain as the most abundant surface intermediates. In contrast, the rate constants for pathway 2 decrease with increasing alkanal size, because larger alkanals exhibit lower hydride ion affinities and thus are less effective toward hydride ion abstraction. The reactivities of the secondary alkenal cyclization−dehydration reactions increase with molecular size, because larger alkyl substitution at the C═C position of the alkenals increases the electron density of the C═C bond and thus promotes the intramolecular electrophilic attack of the carbonyl group onto the C═C bond to initiate the cyclization−dehydration reactions. This mechanistic knowledge on the tandem catalytic cycles and their kinetic and thermodynamic requirements provide the framework for rationalizing and then predicting the site time yields for larger oxygenates and hydrocarbons during alkanal deoxygenation turnovers.

■ ASSOCIATED CONTENT

Ⓢ Supporting Information

The Supporting Information is available free of charge on the ACS Publications website at DOI: 10.1021/acscatal.6b01832.

(PDF)

■ AUTHOR INFORMATION

Corresponding Author

*Y.-H.C.C.: e-mail, cathy.chin@utoronto.ca; tel, (416) 978-8868; fax, (416) 978-8605.

Notes

The authors declare no competing financial interest.

■ ACKNOWLEDGMENTS

This study was supported by Natural Sciences and Engineering Research Council of Canada (NSERC), Valmet, Abellon CleanEnergy, Ontario Early Researcher Award Program, Canada Foundation for Innovation (CFI); F.L. acknowledges a Hatch Graduate Scholarship for Sustainable Energy Research and Ontario Graduate Scholarship for support.

■ REFERENCES

(1) Oasmaa, A.; Kuoppala, E.; Gust, S.; Solantausta, Y. *Energy Fuels* **2003**, *17*, 1−12.

(2) Valle, B.; Gayubo, A. G.; Aguayo, A. T.; Olazar, M.; Bilbao, J. *Energy Fuels* **2010**, *24*, 2060−2070.

(3) Zhang, Q.; Chang, J.; Wang, T.; Xu, Y. *Energy Convers. Manage.* **2007**, *48*, 87−92.

(4) Gayubo, A. G.; Aguayo, A. T.; Atutxa, A.; Aguado, R.; Bilbao, J. *Ind. Eng. Chem. Res.* **2004**, *43*, 2610−2618.

(5) Gayubo, A. G.; Aguayo, A. T.; Atutxa, A.; Aguado, R.; Olazar, M.; Bilbao, J. *Ind. Eng. Chem. Res.* **2004**, *43*, 2619−2626.

(6) Adjaye, J. D.; Bakhshi, N. N. *Fuel Process. Technol.* **1995**, *45*, 161−183.

(7) Jae, J.; Tompsett, G. A.; Foster, A. J.; Hammond, K. D.; Auerbach, S. M.; Lobo, R. F.; Huber, G. W. *J. Catal.* **2011**, *279*, 257−268.

(8) Hoang, T. Q.; Zhu, X.; Sooknoi, T.; Resasco, D. E.; Mallinson, R. G. *J. Catal.* **2010**, *271*, 201−208.

(9) Hoang, T. Q.; Zhu, X.; Lobban, L. L.; Resasco, D. E.; Mallinson, R. G. *Catal. Commun.* **2010**, *11*, 977−981.

(10) Dumitriu, E.; Hulea, V.; Fechete, I.; Auroux, A.; Lacaze, J.-F.; Guimon, C. *Microporous Mesoporous Mater.* **2001**, *43*, 341−359.

(11) Lin, F.; Chin, Y.-H. *J. Catal.* **2014**, *311*, 244−256.

(12) Komatsu, T.; Mitsuhashi, M.; Yashima, T. In *Aldol Condensation Catalyzed by Acidic Zeolites*; 2nd International Conference of the Federation-of-European-Zeolite-Associations, Taormina, Italy, Sept 01−05, 2002; Aiello, R.; Giordano, G.; Testa, F., Eds.; Federation-of-European-Zeolite-Associations: Taormina, Italy, 2002; pp 667−674.

(13) Santilli, D. S. *J. Catal.* **1986**, *99*, 327−334.

(14) Hoelderich, W.; Merger, F.; Mross, W. D.; Fouquet, G. *Preparation of Dienes by Dehydration of Aldehydes*. U.S. Patent US4560822 A, 1985.

(15) Wideman, L. G.; Ohio, T. *Process for the Production of Diene from Aldehydes*. U.S. Patent US4628140, 1986.

(16) Hudson, I. D.; Hutchings, G. J. *Preparation of Conjugated Dienes*. U.S. Patent US5264644 A, 1993.

(17) Hutchings, G. J.; Hudson, I. D.; Bethell, D.; Timms, D. G. *J. Catal.* **1999**, *188*, 291−299.

(18) Lin, F.; Chin, Y.-H. *J. Catal.* **2016**, *341*, 136−148.

(19) Yang, Y.; Lin, F.; Chin, Y.-H. *Chem. Cat. Chem.*, submitted for publication.

(20) Scanlon, J. T.; Willis, D. E. *J. Chromatogr. Sci.* **1985**, *23*, 333−340.

(21) Aihara, J.-i. *J. Chem. Soc., Perkin Trans. 2* **1996**, 2185−2195.

(22) Kozhevnikov, I. V.; Sinnema, A.; van Bekkum, H. *Catal. Lett.* **1995**, *34*, 213−221.

(23) Kubelková, L.; Cejka, J.; Novakova, J. *Zeolites* **1991**, *11*, 48−53.

(24) Solans-Monfort, X.; Bertran, J.; Branchadell, V.; Sodupe, M. *J. Phys. Chem. B* **2002**, *106*, 10220−10226.

(25) Xu, M.; Wang, W.; Hunger, M. *Chem. Commun.* **2003**, 722−723.

(26) Bosacek, V.; Kubelkova, L. *Zeolites* **1990**, *10*, 64−65.

(27) Florian, J.; Kubelkova, L. *J. Phys. Chem.* **1994**, *98*, 8734−8741.

(28) Migues, A. N.; Vaitheeswaran, S.; Auerbach, S. M. *J. Phys. Chem. C* **2014**, *118*, 20283−20290.

(29) Hanna, D. G.; Shylesh, S.; Li, Y.-P.; Krishna, S.; Head-Gordon, M.; Bell, A. T. *ACS Catal.* **2014**, *4*, 2908−2916.

(30) Boronat, M.; Viruela, P.; Corma, A. *J. Phys. Chem. A* **1998**, *102*, 9863−9868.

(31) Boronat, M.; Viruela, P.; Corma, A. *J. Phys. Chem. B* **1999**, *103*, 7809−7821.

(32) Kazansky, V. B.; Frash, M. V.; van Santen, R. A. *Catal. Lett.* **1997**, *48*, 61−67.

(33) Mullen, G. M.; Janik, M. J. *ACS Catal.* **2011**, *1*, 105−115.

(34) Kawakami, H.; Yoshida, S. *J. Chem. Soc., Faraday Trans. 2* **1986**, *82*, 1385−1397.

(35) Baines, D. A.; Jones, R. A.; Webb, T. C.; Campion-Smith, I. H. *Tetrahedron* **1970**, *26*, 4901−4913.

(36) Clark, B. C., Jr; Powell, C. C.; Radford, T. *Tetrahedron* **1977**, *33*, 2187−2191.

(37) Kimura, K.; Nishimura, H.; Iwata, I.; Mizutani, J. *J. Agric. Food Chem.* **1983**, *31*, 801−804.

(38) Price, C. C.; Dickman, M. L. *Ind. Eng. Chem.* **1948**, *40*, 257−261.

(39) Loori, J. J.; Cover, A. R. *J. Food Sci.* **1964**, *29*, 576−582.

(40) Cheng, H.; Meng, X.; Liu, R.; Hao, Y.; Yu, Y.; Cai, S.; Zhao, F. *Green Chem.* **2009**, *11*, 1227−1231.

(41) Bradsher, C. K. *Chem. Rev.* **1946**, *38*, 447−499.

(42) Bradsher, C. K.; Vingiello, F. A. *J. Am. Chem. Soc.* **1949**, *71*, 1434−1436.

(43) Bradsher, C. K. *Chem. Rev.* **1987**, *87*, 1277−1297.

(44) Bradsher, C. K. *J. Am. Chem. Soc.* **1942**, *64*, 1007−1007.

(45) Dias, J. A.; Rangel, M. d. C.; Dias, S. C. L.; Caliman, E.; Garcia, F. A. C. *Appl. Catal., A* **2007**, *328*, 189−194.

(46) Sulikowski, B.; Rachwalik, R. *Appl. Catal., A* **2003**, *256*, 173−182.

(47) Dumitriu, E.; Hulea, V.; Kaliaguine, S.; Huang, M. M. *Appl. Catal., A* **1996**, *135*, 57−81.

(48) Apeloig, Y.; Arad, D.; Rappoport, Z. *J. Am. Chem. Soc.* **1990**, *112*, 9131−9140.

(49) Chiang, Y.; Kresge, A. J.; Walsh, P. A. *J. Am. Chem. Soc.* **1982**, *104*, 6122−6123.

(50) Keeffe, J. R.; Kresge, A. J.; Schepp, N. P. *J. Am. Chem. Soc.* **1990**, *112*, 4862−4868.

(51) Kemp, D. S.; Frank, V. *Organic Chemistry*; Worth Publishers: New York, 1980; pp 839−845.

(52) Noack, W. E. *Theor. Chim. Acta* **1979**, *53*, 101−119.

(53) De Moor, B. A.; Reyniers, M.-F.; Gobin, O. C.; Lercher, J. A.; Marin, G. B. *J. Phys. Chem. C* **2011**, *115*, 1204−1219.

(54) Newalkar, B. L.; Choudary, N. V.; Kumar, P.; Komarneni, S.; Bhat, T. S. G. *Chem. Mater.* **2002**, *14*, 304−309.